DELOS EVK3-CT-2000-00041

Wave Action on Rubble Mound Breakwaters: the Problem of Scale Effects

Matteo Tirindelli & Alberto Lamberti (University of Bologna)
Doros Paphitis & Michael Collins (University of Southampton)
Cesar Vidal (University of Cantabria)
Stephen Hawkins & Paula Moschella (MBA)
Hans Burcharth (Aalborg University)
Agustin Sanchez-Arcilla (Politecnical University of Catalunia)

Contents

1. Introduction 3

2. Properties of Sea Water 3
2.1 General 3
2.2 Sound speed 5

3. Scaling Laws 7
3.1 Froude number and scaling law 7
3.2 Reynolds number and scaling law 7
3.3 Weber number and scaling law 7
3.4 Cauchy number and scaling law 8
3.5 Main mechanisms affecting scaling laws 9

4. Surface Tension Effects on Breakers 9
4.1 General 9
4.2 Breaking waves 9

5. Air Content 10
5.1 Air entrapment/entrainment and bubble formation 11
5.2 Air escape 12
5.3 Processes of bubble formation in fresh and sea water 13
5.4 Compression of air 16

6. Scale Effects Related to Wave-Structure Interactions 17
6.1 Wave impacts on armour units 17
6.2 Run-up and overtopping 20
6.3 Structure Deformation 20
6.4 Porous flow 20
6.5 Flow forces on plants and organisms 21

7. Movale-Bed Scale Effects 21
7.1 Generalities 21
7.2 Hydrodynamic and sediment parameters 21
7.3 Bedload-dominated transport models 24
7.4 Suspended load-dominated transport models 25

7.5 Scour at the trunk section 25
7.6 Overview on scale effects on sediment transport 26

8. Effects of Marine Growth on Rubble Mound Breakwaters 27

9. Conclusions 29

Selected References 32

Appendix 1: Surface Tension Effects on Waves 37
A1.1 Surface tension and free surface boundary conditions 37
A1.2 Effects of surface tension on linear waves 38
A1.3 Effect of surface tension on turbulent free surface flow 40

Appendix 2: Effects of Surface Tension on Breaking Waves 43

Appendix 3: Experimental Approaches to Scale Effects Associated to Wave Impacts ... 49

Appendix 4: Boundaries for Sound Speed 51

Appendix 5: Further References 53

1. Introduction

The present report, produced within the framework of the EU funded project DELOS, attempts to recognise and analyse main scale effects in the physical modelling of rubble mound breakwaters used in offshore and coastal engineering. Scale effects appear in physical modelling because the ratios between the forces of interest, as present in prototype, cannot be maintained in a scaled model. The report is by no means intended to resolve the problems associated with scale effects, given the complexity of this issue. However this discussion provides a preliminary understanding of these effects.

Respect to the aforementioned objectives, the present report is structured as follows. The properties of sea water are summarised in Section 2. Section 3 provides a brief overview of scaling rules used in hydraulic physical modelling. Section 4 is dedicated to surface tension effects on breakers. Section 5 deals with the complex problem of scaling air content from prototype sea water to model fresh water. A general overview of main scale effects in relation to the different processes associated to the interaction between waves and rubble mound breakwaters is presented in Section 6. Scaling of movable-bed models are addressed in Section 7. The effects of marine organisms on water and mound units are described in Section 8. In Section 9 conclusions are drawn, which summarise the main points worth considering when addressing the problem of scale effects in wave-related models with rubble mound breakwaters. Selected issues are further discussed in the attached appendices.

2. Properties of Sea Water

2.1 General

Sea water is a binary fluid in that it consists of various salts, whose presence affects a number of oceanic parameters including sound speed, compressibility, refractive index, thermal expansion and others.

Temperature is basic to any physical description of the ocean. Temperature varies strongly in the upper layers of the ocean, and with it, other properties dependent on it: density, sound speed, surface tension, viscosity, etc.

The compressibility of sea water can be expressed by the coefficient of compressibility, which relates fractional changes in water volume to the corresponding changes in pressure (i.e. Apel, 1987). Compressibility of sea water is an important factor in several applications, including: precise determination of sea water density; computation of adiabatic temperature changes; computation of sound speed in sea water and it affects the characteristics of eventual wave-induced impacts on maritime structures.

Density of sea water is related to temperature, salinity and pressure (which is nearly linearly proportional to depth) through the equations of state; it provides a measure of the hydrostatic stability in the ocean (see Fig. 1). Sea water contains several salts in suspension, among which the most important are Sodium and Magnesium chlorides and sulphates. Total content of salt in sea water is generally between 33 and 38 $g/Kg_{seawater}$. A typical distribution of ions is shown in Table 1.

Ion	**Concentration [g/Kg]**
Cl^-	18.970
SO_4^{--}	2.650
HCO_3^-	0.140
Br^-	0.065
F^-	0.001
H_2BO_3	0.026
Na^+	10.470
Mg^{++}	1.280
Ca^{++}	0.410
K^+	0.380
Sr^{++}	0.013
Total	34.40

Table 1. Components of sea water.

Chlorides, bromides and iodides provide a measure for "Chlorinity" (*Cl*, [g/Kg$_{solution}$]), from which values of salinity *S* [g/Kg] can be derived through:

$$S = 0.03 + 1.805\ Cl \qquad (1)$$

An empirical relation between *S* and the environmental processes which control it is the following:

$$S = 34.60 + 0.0175\ (E\text{-}P) \qquad (2)$$

where (*E-P*) is Evaporation - Rainfall [cm/year].

Surface sea water density depends on temperature and salinity, see Figure 1.

Average surface sea water salinity is around 35 g/Kg.

Density and osmotic pressure increase with salinity, respectively 0.8 Kg/m^3 and 0.65 bar for each g/Kg.

Solidification temperature and steam tension decrease with increasing salinity, respectively -0.055 °C and -0.054% for each g/Kg.

Compressibility is slightly lower (10%) than in fresh water.

Cinematic viscosity is slightly higher (4%).

Specific heat and heat conductivity decrease with salinity and at average salinity, they are respectively 7% and 4% lower than corresponding fresh water values.

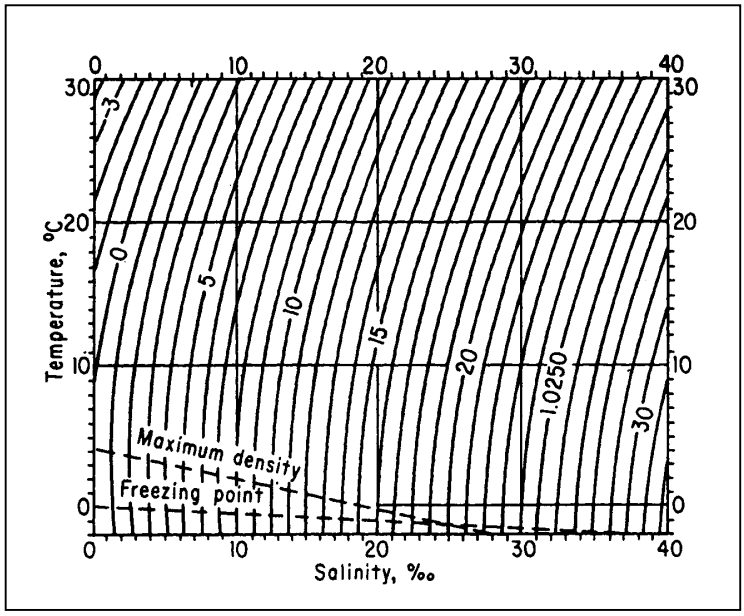

Figure 1. Surface sea water density as a function of temperature and salinity

Parameter		Unit	Value	Ratio to fresh water
Density	0 °C	Kg/m^3	1028.1	1.0282
	10 °C		1027.0	1.0272
	20 °C		1024.8	1.0266
	30 °C		1021.8	1.0262
Viscosity	0 °C	10^{-6} m^2/s	1.975	1.024
	10 °C		1.356	1.037
	20 °C		1.056	1.049
	30 °C		0.853	1.061
Surface tension	0 °C	Kg/s^2	76.4	1.01
	30 °C		72.2	1.01
Cubic compressibility modulus	0 °C	10^9 Kg/m/s^2	2.20	1.090
	30 °C		2.50	1.088
Specific heat at constant pressure	0 °C	cal/g/°C	0.941	0.934
	30 °C		0.929	0.931
Heat conductivity	18 °C	cal/m/s/°C	0.134	0.958

Table 2. Physical characteristics of sea water at S = 35 g/Kg and p = 1 bar.

2.2 Sound speed

Speed of sound, in sea and fresh water, constitutes one of the factors that need consideration in any modelling investigation. In order to deal with the scale effects related to sound speed, an improved understanding of the behaviour of sound in spatially complex and temporally variable acoustic mediums is required. Acoustical oceanography describes the role of the

ocean as an acoustic medium, relating oceanic properties to the behaviour of underwater acoustic propagation, noise and reverberation. The speed of sound represents the single most important acoustic variable in the ocean, whose distribution influences all the other acoustic phenomena.

Speed of sound (c) in sea water is related to isothermal compressibility ($K \equiv d\rho/(\rho \cdot dp)$) through the following:

$$c = \sqrt{\frac{\gamma}{K\rho}} \tag{3}$$

where γ is the ratio of specific heats at constant pressure and volume, and ρ is the density of sea water.

The speed of sound in sea water is an oceanographic variable that determines the behaviour of sound propagation and varies (proportionally) as a function of water temperature, salinity and pressure. Many empirical relationships have been developed over the years for calculating sound speed using values of water temperature, salinity and pressure. Frequently used formulae include those of Wilson (1960), Leroy (1969), Frye & Pugh (1971), Del Grosso (1974), Mackenzie (1981) Spiesberger & Metzger (1991) and Dushaw *et al.* (1993). Each formula has its own limits for temperature, salinity and pressure. The formula developed by Mackenzie (1981) is presented below.

$$c = 14448.96 + 4.591T - 5.304\ 10^{-2}T^2 + 2.374\ 10^{-4}\ T^4 + 1.340\ (S\text{-}35) + 1.630\ 10^{-2}\ D +$$
$$+ 1.675\ 10^{-7}\ D^2 - 1.025\ 10^{-2}\ T\ (S\text{-}35) - 7.139\ 10^{-13}\ T\ D^3 \tag{4}$$

where c is in m/s, T is temperature (°C), S is salinity (‰) and D is depth (m). This equation is valid over the following ranges: 0°C≤T≤30°C; 30‰≤S≤40‰; 0≤D≤8000m.

Sound propagates in the sea through a variety of paths which depend upon sound speed structure in the water column and geometry of the receiver. These paths are (see Figure 2): direct path; surface duct; bottom bounce; convergence zone; deep sound channel; reliable acoustic path. Various combinations of paths are also possible and are referred to as multi-path propagation.

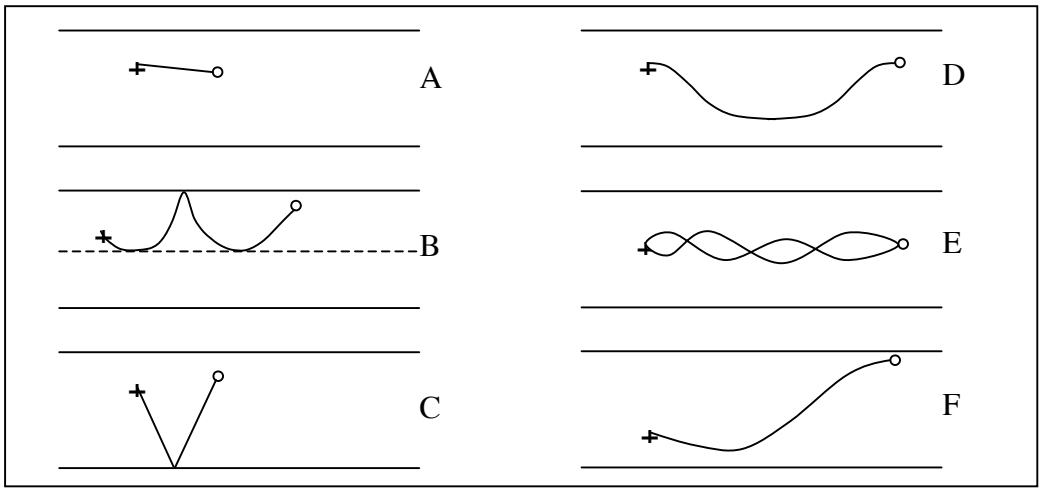

Figure 2. Six basic propagation paths in the sea: A – direct path; B – surface duct; C – bottom bounce; D – convergence zone; E – deep sound channel; F – reliable acoustic path (adopted from Etter, 1996).

3. Scaling Laws

Forces to be considered are: inertia; gravity; viscous; elastic; surface tension.

Inertia forces are always present in flows related to waves. Ratios between inertia and other types of force appear as independent dimensionless coefficients in the non-dimensional equations of motion. The most relevant coefficients for model studies related to DELOS project are described below.

3.1 Froude number and scaling law

$$Fr \equiv \frac{U}{\sqrt{gl}} \tag{5}$$

is the square root of the ratio between inertia and gravity forces.

Data deriving from physical models in which wave action is the dominant force are usually converted to prototype scale by use of Froude law.

Gravity and most fluid characteristics are almost equal in model and prototype, therefore, if the contrary is not explicitly stated, it can be assumed that they are maintained.

For any variable *X*, let n_X be the ratio among corresponding variables in prototype and model: $n_X = X_p / X_m$.

Maintaining Froude number in model and prototype ($n_{Fr} = 1$), the following expressions for time (*t*), velocity (*U*) and pressure (*p*) scales can be derived:

$$n_t = n_U = n_l^{1/2} \tag{6}$$

$$n_p = n_l \tag{7}$$

3.2 Reynolds number and scaling law

$$Re \equiv \frac{Ul}{\nu} \tag{8}$$

is the ratio between inertia and viscous forces. Maintaining Reynolds number, the following expressions for scaling time, velocity and pressure scales can be derived:

$$n_t = n_l^2 \tag{9}$$

$$n_U = n_l^{-1} \tag{10}$$

$$n_p = n_l^{-2} \tag{11}$$

3.3 Weber number and scaling law

$$We \equiv \frac{\rho U^2 l}{\sigma} \tag{12}$$

is the ratio among inertia and surface tension forces, an important parameter to be taken in account when air entrainment or surface tension are relevant processes. In these cases the ratio should be preserved leading to Weber scaling law. Surface tension can be easily altered by a small amount of natural or artificial surfactants; differences in this parameter are therefore explicitly accounted for.

The following expressions for time, velocity and pressure scales can be derived.

$$n_t = n_\sigma^{-1/2} \cdot n_l^{3/2} \tag{13}$$

$$n_U = n_\sigma^{1/2} \cdot n_l^{-1/2} \tag{14}$$

$$n_p = n_\sigma \cdot n_l^{-1} \tag{15}$$

3.4 Cauchy number and scaling law

$$Ca \equiv \frac{\rho U^2}{E} \tag{16}$$

is the ratio between inertia and elastic forces ($E \equiv dp/(d\rho/\rho) = 1/K$), it is related to Mach number, that is the ratio among particle velocity and sound celerity.

$$Ma \equiv \frac{U}{c} = \frac{U}{\sqrt{E/\rho}} \tag{17}$$

The presence of a mixture of air and water, even when the quantity of air is extremely reduced, causes the liquid to be much more compressible than water alone. When pressure variation is very high, changes in air density may be important. In such cases, pressure density relationship becomes non linear and a single compressibility coefficient does not apply to the full compression process. When the compressibility is the dominant factor, conversion to prototype should be made by using Cauchy law. The elasticity of air-water mixtures depends on air content, that may be significantly different in prototype and model, and on ambient pressure, that does not scale as a small pressure perturbation (see Section 5.4) and therefore, the effect of elasticity scale is expressly represented.

Maintaining Cauchy or Mach number, the following expressions for scaling time, velocity and pressure can be derived.

$$n_t = n_E^{-1/2} \cdot n_l \tag{18}$$

$$n_U = n_E^{1/2} \tag{19}$$

$$n_p = n_E \tag{20}$$

In the relations above, ρ is water density, U is a characteristic flow velocity, l is a characteristic length, g is gravitational acceleration, ν is cinematic viscosity, σ is surface tension, E is elasticity/compressibility modulus, K is bulk modulus of the fluid and c is speed of sound.

3.5 Main mechanisms affecting scaling laws

The ratio between ***inertia*** and ***gravity*** forces (expressed by Froude number) is essential in any wave hydraulic model, to assure the scale reproduction of waves. The effect of ***viscous*** damping, in conventional reproduction of non-breaking laboratory waves, is negligible if water depths are greater than 2-3 cm and wave propagation is over a short distance. ***Surface tension*** can cause some scale effects on non-breaking laboratory wave propagation, but only if laboratory waves are very small and steep, i.e. heights and periods below 2cm and 0.3s, respectively; however, in breaking waves surface tension causes a scale effect on air entrainment (more details on surface tension effects are given in Section 4). ***Compressibility*** of air-water mixture is much different in prototype or model conditions and therefore, causing an important scale effect (see Section 5.4).

In general, as it will be explained further in this report, none of the above scaling laws provides accurate scaling for all processes in wave-related breakwater models. Main scale effects from prototype to model are due to: intrinsic properties of the fluid that do not scale appropriately (viscosity, surface tension, air content etc.); interaction with compliant structures; qualitative differences in processes in field and laboratory (obstruction of pores by algae and mussels in sea-water, reduced coalescence of air bubbles in sea-water) and different scaling used for water and sediment in mobile bed tests.

4. Surface Tension Effects on Breakers

4.1 General

The kinematic description of breaking waves is frequently based on data obtained from laboratory experiments. The scaling of these results to real life is normally carried out using Froude law, therefore, neglecting the effects of viscosity and surface tension. In this report, the effects of surface tension on breaking waves is addressed based mostly on the publications of Duncan (2000), Perlin & Schultz (2000) and Melville (1996)

4.2 Breaking waves

When waves increase their steepness, the mean curvature radius in the crest decreases, thus increasing the surface-tension effects. Stokes (1880) analysis of deep-water periodic waves of maximum amplitude predicted a maximum wave steepness of $ak = 0.4432$ ($a = H/2$ or wave amplitude) with a sharp crest forming an angle between forward and backward slopes of 120º.

This finding has been considered in the past as a model for breaking. Recently, considering Benjamin-Feir instability mechanism it was shown that even waves having much milder steepness down to approximately 0.2 can develop breakers if enough space is provided.

Surface tension and viscosity have effects particularly near the sharp crest of a breaking wave, see Figure 3; therefore criteria of breaking based on steepness or slope, consistent with Froude scaling, if valid at all, do not represent the effects of surface tension and viscosity and may result in scale-dependent breaker shape and breaking indexes if wave length is less than 0.5 m or mean frequency greater than 2 Hz. Elasticity can also play an important role in some of the breaking stages.

More information on surface tension effects on waves and related scale effects can be found in Appendices 1 and 2.

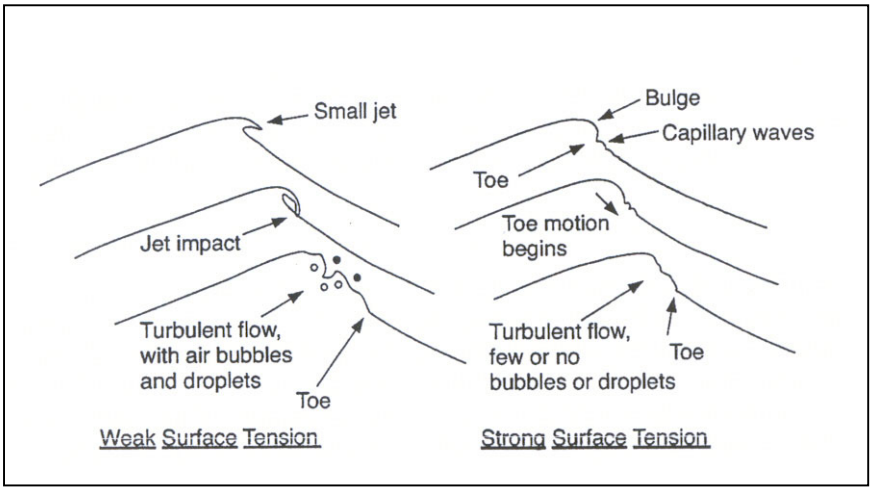

Figure 3. Schematic showing three phases of spilling breaking for weak and strong surface tension effects (after Duncan, 2000).

5. Air Content

In general, the air in a breaker curl or between a structure and an approaching wave may be ***expelled***, ***entrapped*** **or** ***entrained***.

Air is said to be expelled if it remains a connected body above the water. If the air is expelled no significant mixture of air and water takes place, pressures do normally rise slowly (pulsating pressure varying at wave frequency) and, if this is the case, Froude scaling law does apply. Air is said to be entrapped if the plunging jet separates entrapping air ; pressure in entrapped air may be quite different from free air pressure. Often entrapped air is compressed and partially entrained. Air is entrained in the water column as a result of breakers, whether spilling or plunging, in the form of bubbles (Figure 4).

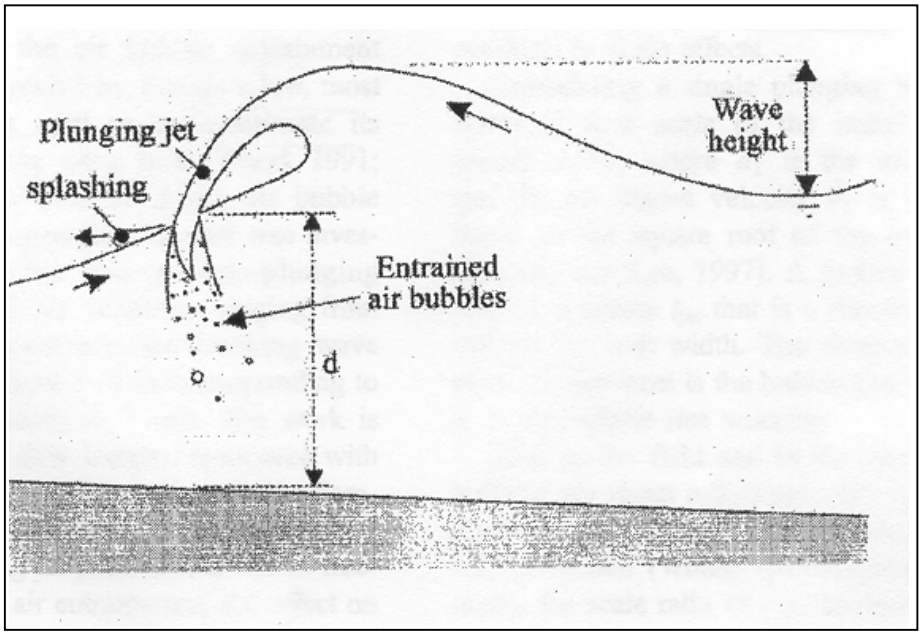

Figure 4. Plunging breaking wave (after Chanson *et al.*, 2002).

5.1 Air entrapment/entrainment and bubble formation

In the case when a significant quantity of air is enclosed within a wave or between a wave and structural boundaries (as for the case of a plunging breaker over a rubble mound breakwater), the air is said to be ***entrapped***. If the impact is sufficiently violent, the air pocket subdivides, and many of the resultant bubbles remain ***entrained*** in the water for a time varying from a fraction of wave period to several wave periods.

Bubbles form in a variety of sizes ranging normally from 10μm to 10cm. The most frequent diameters of bubbles, entrained after a breaker, are in the 20-30μm size range. The total volume of air in a unit volume of mixture is known as the "void ratio" (β).

The presence of air alters both mixture density and compressibility:

$$\rho_m = (1-\beta)\cdot \rho_w + \beta \cdot \rho_a$$

$$K_m = (1-\beta)\cdot K_w + \beta \cdot K_a$$

Density ratio of air and water is 1/800; compressibility ratio is 20'000/1. The resulting celerity of low frequency compression waves (not resonating with bubbles) does not vary monotonously from water celerity (≅1500m/s) to air celerity (≅330m/s), but falls down to a minimum at about 20m/s for an air void fraction ranging from 0.1% to 1% (Wood, 1941).

The presence of entrapped/entrained air has a sort of "cushioning" effect with respect to the impulsive loading. Maximum pressure is reduced and rise time increased because of aerated water. This trend increases with the rate of air present in the water and the violence of impact (Figure 5; data relative to drop tests). In the plot, Pressure Reduction Factor (*PRF*) is defined as the ratio between maximum pressure recorded in an experiment with aerated water and the average of the corresponding maximum pressure recorded with unaerated water ($\beta = 0$).

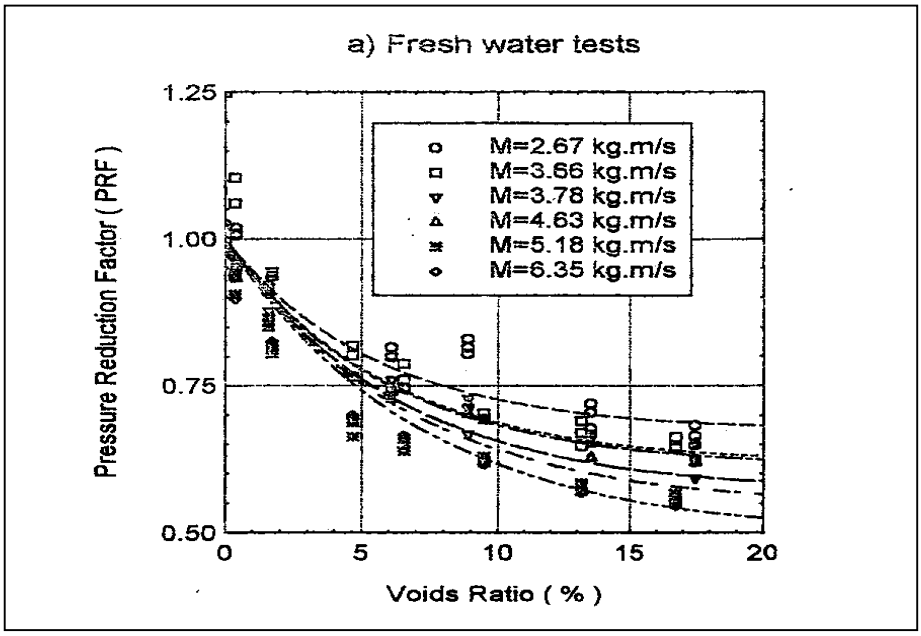

Figure 5. Variation of Pressure Response Factor with void ratio β and violence of impact (after Bullock *et al*, 2001).

5.2 Air escape

Entrained air escapes from water either as rising bubbles, that eventually reach the free surface, or by dissolving into sea water. The different dimensions of bubbles influence their rise velocity, their capillary excess pressure and dissolution rate. The greater the bubbles, the quicker they rise and escape from water. Small to medium bubbles in sea water have the tendency to slow down their rise velocity to values typical of Stokes law (Slauenwhite & Johnson, 1996). Chanson *et al.* (2002) reviewed the different formulae used for calculating rise velocity. They report three different equations for different bubble diameter ranges:

$$v_r = \frac{2}{9} \cdot \frac{g \cdot (\rho_w - \rho_a)}{\mu_w} \cdot d_{ab}^{\ 2} \qquad \text{for } d_{ab} < 0.1\text{mm} \qquad (21)$$

$$v_r = \frac{g}{18} \cdot \frac{\rho_w}{\mu_w} \cdot d_{ab}^{\ 2} \qquad \text{for } 0.1\text{mm} < d_{ab} < 1\text{mm} \qquad (22)$$

$$v_r = \sqrt{\frac{2.14 \cdot \sigma}{\rho_w \cdot d_{ab}} + 0.52 \cdot g \cdot d_{ab}} \qquad \text{for } 1\text{mm} < d_{ab} \qquad (23)$$

where subscripts $_w$ and $_a$ refers to air and water, $_{ab}$ stands for air bubble, d is bubble diameter, σ is surface tension between air and water, μ is dynamic viscosity. Figure 6 shows a plot of v_r versus bubble radius according to formulae of Equations 22 and 23 (in the range d_{ab} > 0.1mm).

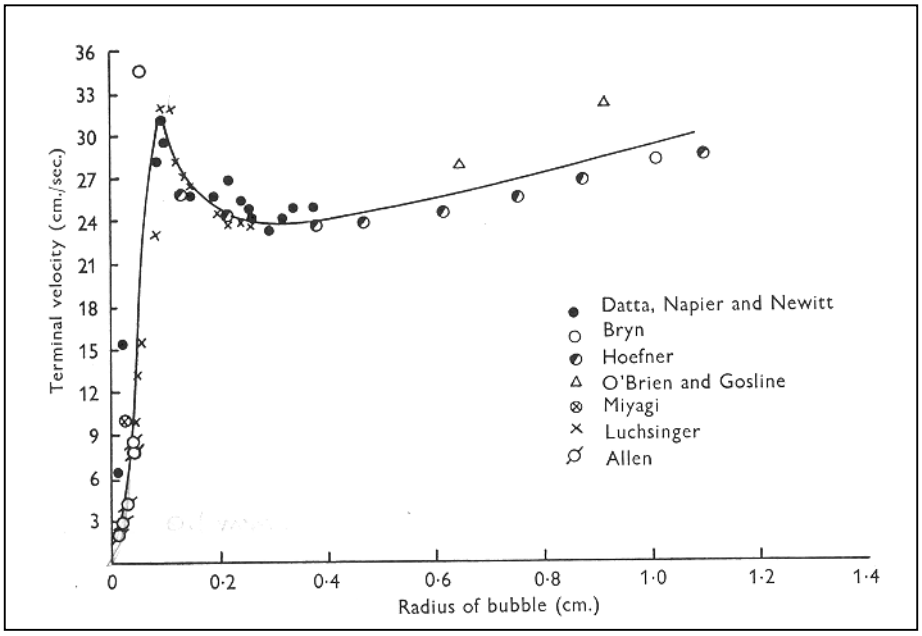

Figure 6. Rise velocity vs. bubble radius (after Datta *et al*, 1950).

The very small bubbles dissolve rapidly into water. For diameter not greater than 0.4 mm bubble shape remain spherical and the bubble rises vertically with a uniform velocity. For diameter in the range 0.4-4.0 mm bubbles assume an ellipsoidal shape with the longer axis horizontal and travel upwards following a zigzag path. Bubbles greater than 4.0 mm become unstable when rising, they assume irregular shape and follow irregular paths. For the larger sizes disruption may occur with the formation of small satellite bubbles.

5.3 Processes of bubble formation in fresh and sea water

The process of air entrainment is highly dependent on water characteristics. It is recognised that temperature, salt concentration, ionic structure, surface tension, viscosity, and exudates of marine organisms play an important role in number and size distribution of bubble population. Slauenwhite & Johnson (1999) explored in detail the different mechanisms of bubble formation in sea and fresh water. They found that sea water bubbles are generally 4-5 times as many as in fresh water for similar generation conditions and generally smaller (Figures 7 and 8).

Fresh water bubbles have a greater tendency to coalesce and escape from water because of buoyancy. Tendency to coalescence is inhibited by ionic structure of sea water and by presence of plankton and/or marine exudates (Craig *et al.,* 1993). Therefore, at a given level of entraining agent intensity, the number of (small) bubbles (and the air content) in sea water is higher than in fresh water (Haines & Johnson, 1995). These bubbles are small in dimensions and they find it very difficult to escape, leading to persistence and to a general increase in ambient level of aeration in sea water with respect to fresh water.

This is also confirmed by Monahan & Zietlow (1969), who performed laboratory whitecaps simulations, finding that saltwater whitecaps areas decay exponentially with a higher time constant than fresh water. Figure 7 shows a distribution of bubbles in fresh and sea water under identical macroscopic conditions. It can be noted that for a given bubble radius, the number of bubbles in sea water is higher than in fresh water.

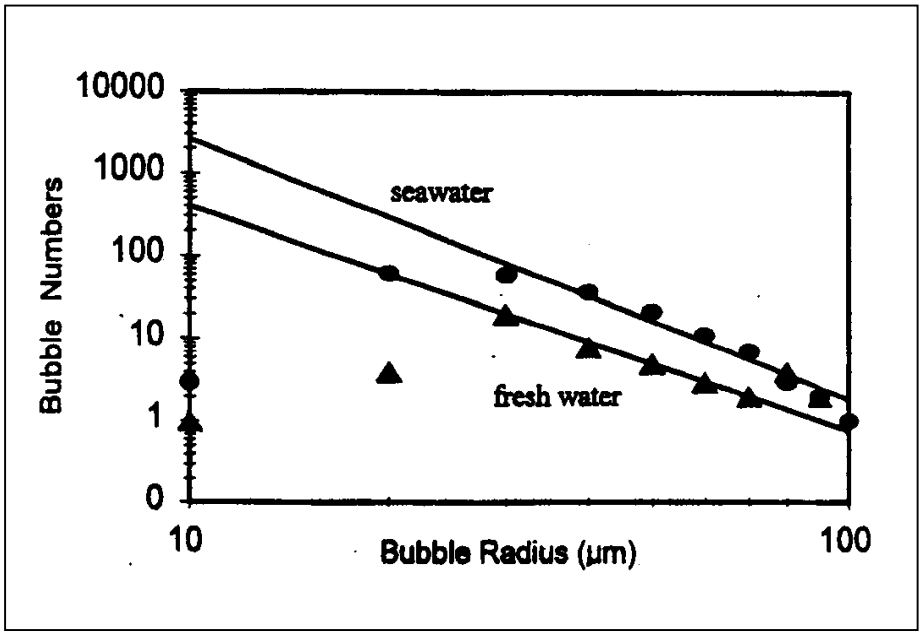

Figure 7. Distribution of bubbles in fresh and sea water (after Slauenwhite & Johnson, 1999).

Cartmill and Su (1993) analysed some large scale tests in a wave flume with breaking waves and found that small size bubble number(for $30\mu \leqslant r \leqslant 800\mu$) is up to 10 times higher in saltwater than in freshwater (20‰ against 2‰).

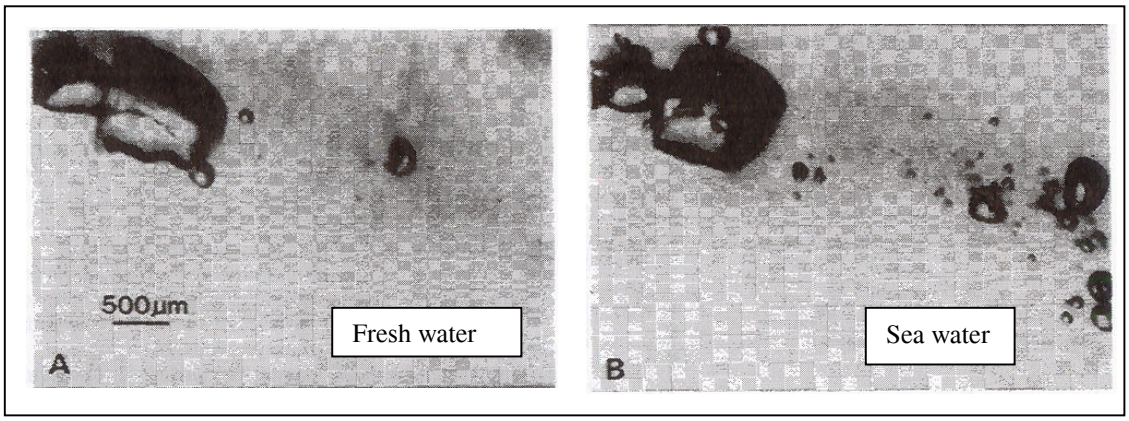

Figure 8. Examples of bubble sizes for entrained air in fresh and sea water (after Slauenwhite & Johnson, 1999).

Bullock *et al.* (2001) conducted some tests by artificially aerating fresh water and sea water. They confirm that the process of bubble formation is rather different from sea water to fresh water. In fresh water a higher number of large bubbles tend to form than in sea water (Figure 9). The largest bubbles escape from fresh water breakers within a single wave period, whereas in sea water they can persist for several wave periods. This leads to very different aeration levels between fresh and sea water. While in sea water model tests (wave tests, Froude scale 1:25) void ratios (aeration levels) reached values up to 3.9%, in fresh water model tests; these values were one order of magnitude less. The use of fresh water in laboratory can explain some of the differences related to the different environments.

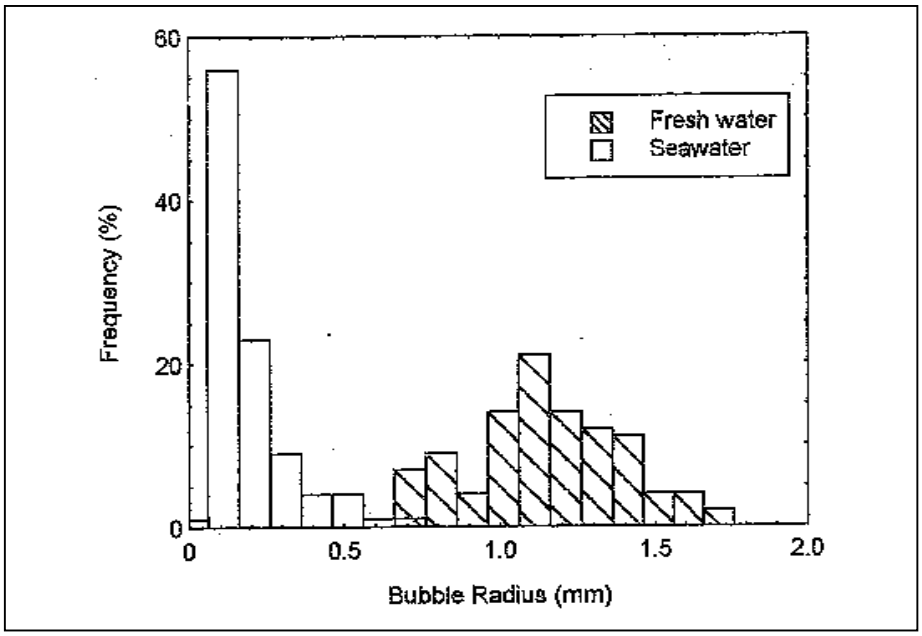

Figure 9. Bubble size distribution in fresh and sea water (after Bullock *et al*, 2001).

Care must be taken, though, because it is impossible to reproduce exactly field conditions in laboratory, due to the presence of marine organisms which behave differently in the real sea

than in laboratory sea water. Bullock *et al.* (2001) reported to have measured values of void ratio of up to 8.4% in field wave breakers. Furthermore, they state that, when comparing the amount of foam generated in sea water laboratory tests of wave impacts due to breaking waves with the amount of foam observed in the field, full scale waves are characterised by higher aeration (they produced higher amount of foam). Aeration is in conclusion subject to a scale effect even when sea water is used in the model.

With this in mind it is important to refer to Su & Wesson (2001), who provided an extensive review of bubble measurement techniques and bubble dynamics in shallow water. They performed a field campaign with the aim to investigate air content of approaching waves to coastal zones. From their paper it is possible to deduce some quantitative information about the different air content of a breaking wave in deep water, in shallow water and of a broken wave. In Figure 10 void fraction variation with time, averaged over a 3-hour period is shown with one standard deviation limits for a breaking wave.

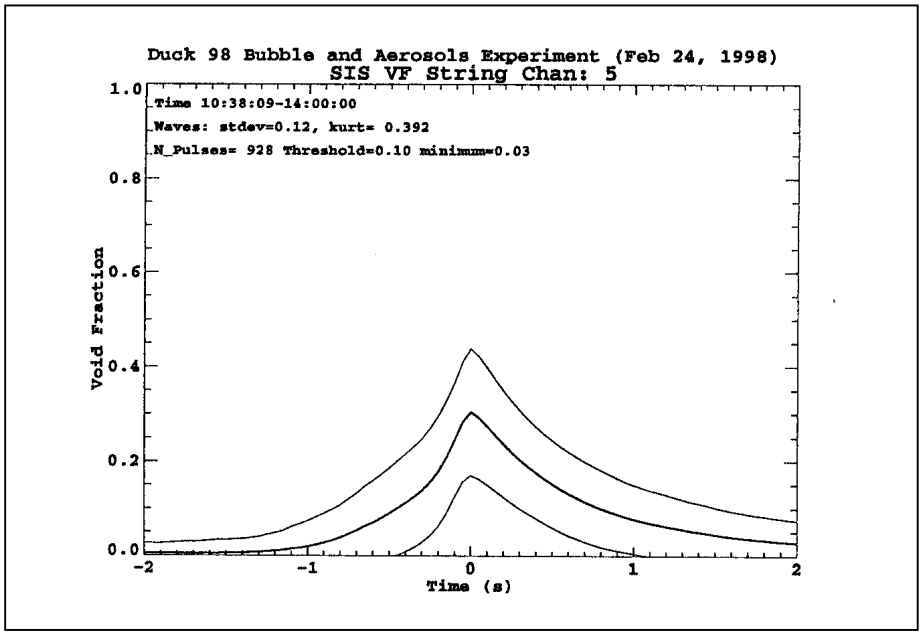

Figure 10. Time variation of void fraction for breaking waves, after Su & Wesson, (2001)

In Figure 11 the hourly averaged void fraction inside and outside the surf zone are shown. Hourly averaged void fraction inside the surf zone (representative of air content of a broken wave) is two magnitude orders higher than its correspondent outside the surf zone (breaking waves in deep water). Air content in deep water breaking waves is strictly dependent on wind speed, whilst in shallow water waves other parameters (mostly wave height) seem to be more relevant. An experimental relation between bubble size density $B(r)$ (in its turn related to void fraction) and wind speed (W) is given as: $\int_{10\mu}^{200\mu} B(r)\,dr \propto W^{4.3}$.

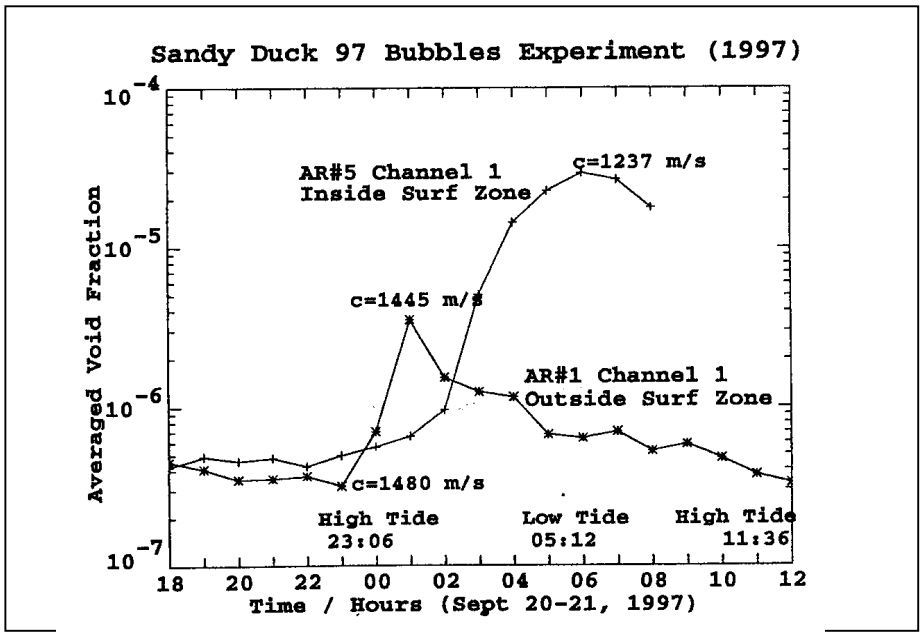

Figure 11. Hourly averaged void fraction in deep and shallow water, after Su & Wesson, (2001)

Summarising, it is possible to estimate values of void fraction for an approaching wave from deep to shallow water with the following:

- Deep water breaking wave - void ratio = 10^{-6}
- Shallow water breaking wave - void ratio = 0.3
- Broken wave - void ratio = 10^{-5}

5.4 Compression of air

Impulsive wave loads are characterised by high shock pressure of very short duration. During this phase, the characteristic velocity of the process is extremely high: the presence of even small amounts of air in the water dramatically influences the process of loading. During impulsive events, compression of air results as a highly non linear process, for which standard law scales prove to be inaccurate for physical modelling.

Bullock *et al* (2001) reported that for laboratory wave tests (Froude scale 1:25), waves with H_s = 0.25 m generated impact pressures of around 10% higher than the corresponding full-scale values generated by breakers of the same prototype size. They also conclude that straightforward Cauchy law scaling can lead to a gross underestimation of maximum pressures and overestimation of rise times.

Considering that inertia forces scale as U^2, also a straightforward use of Weber law would lead to errors, given that $We = \frac{\rho U^2 l}{\sigma}$, and that surface tension does not scale from model to prototype.

Regarding the effect or the non-scaling ambient pressure, the quantity $\int \frac{dp}{\rho}$ could be considered rather than simple pressure. If the flow scales according to Froude and the compression is barotropic, the same scaling applies to the pressure integral. Peregrine & Thais (1996) studied the effect of air entrainment in violent wave impacts. They approach the problem considering a compressible air-water mixture and assuming that the air changes volume according to the polytropic law

$$p_a \rho_a^{-k} = \text{constant} \tag{24}$$

where p_a is air pressure, ρ_a is air density and k is the polytropic index, taken as $k = 1.4$.

Through Equation 23 they derive a state equation for the mixture,

$$\frac{p}{p_1} = \left(\frac{\beta_1}{\beta_1 - \delta} \right)^k \tag{25}$$

where p is the pressure of the mixture, p_1 is the ambient pressure, β_1 is the percentage void fraction, ρ_1 is a reference density of the mixture and δ is 1-(ρ_1/ρ).

Considering Bernoulli Equation,

$$\int \frac{dp}{\rho} + \frac{1}{2} v^2 = \text{constant} \tag{26}$$

where v is the velocity of the mixture air-water, and using Equation 25, the following is obtained:

$$\rho \int_p^{p_1} \frac{dp}{\rho} = p\left(1 + \frac{\beta_1 - \delta \cdot k}{k-1} \right) - \left(\frac{p_1 \cdot \beta_1}{k-1} \right) - p_1 \tag{27}$$

Considering that $\int \frac{dp}{\rho}$ scales with Froude and that p_1 and β_1 do not, it is necessary to know model and prototype values of β_1 (i.e. it is necessary to estimate or measure air content at model and prototype scale).

To sum up, in the cases of wave impacts with significant air content in the water, Froude scaling would generate relevant errors in the evaluation of magnitude and rise time of the loading, and in particular would generate overestimation of maximum pressures, see Peregrine & Thais (1996). Cauchy and Weber laws seem to be inaccurate as well.

6. Scale Effects Related to Wave-Structure Interactions

The interactions considered in this section are: wave impacts on armour blocks; run-up and overtopping; structure deformation; wave generated flow in the porous structure; flow forces on plants and organisms attached to the structure.

6.1 Wave impacts on armour units

In a Froude model there are, in principle, scale effects associated with surface tension, viscous and elastic forces. However, investigations of scale effects in armour stability tests have

shown that if Reynolds number exceeds a certain critical value (Re_c) then the effects are very small. The characteristic flow velocity (U) is often taken as $\sqrt{gH_s}$, where H_s is significant wave height. Several scale effect studies with emerging rubble mound structures have been performed.

- Dai & Kamel (1969) tested rock armour layers with D_{n50} = 20–300 mm and found no scale effects on armour layer damage for $Re_c > 3 \cdot 10^4$ in tests with regular waves.
- Tests by Thompson & Shuttler (1975) with irregular waves and stones in the range of 20–40 mm showed no clear dependence of the erosion on Re.
- Scale effects were studied experimentally in irregular waves by Törum *et al.* (1977), Brodertick & Ahrens (1982), Mol *et al.* (1983), and Van der Meer (1988). No significant scale effect on armour stability was found for Re_c in the range $1\ 10^4$ –$4\ 10^4$.
- Jensen & Klinting (1983) argued from theoretical considerations that $Re_c > 0.7\ 10^4$.
- Sharp & Khader (1984) proposed a value of $Re_c = 4\ 10^5$, whereas Kajima & Sakakiyama (1994) suggested $Re_c = 3\ 10^4$ in tests with regular waves.

A typical wave-induced impact may be considered as two phases. At the instant of contact between the wave and the structure, the ***impulsive force*** is large in magnitude and short in duration. This is followed by a ***pulsating force*** (quasi-static). Examples of force and pressure histories showing the two components described above are shown in Figures 12 and 13.

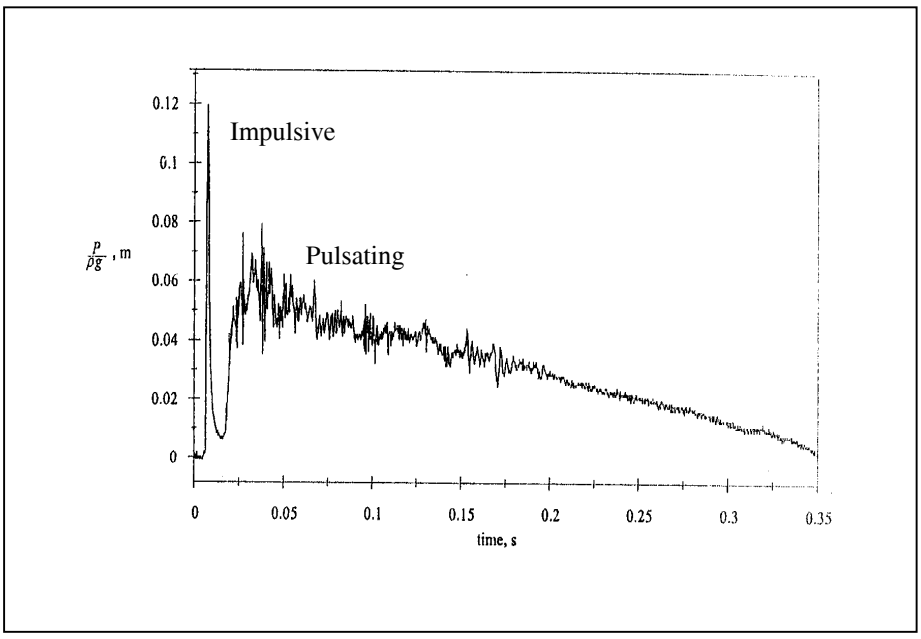

Figure 12. Pressure history on rubble mound slope (after Howarth *et al*, 1996).

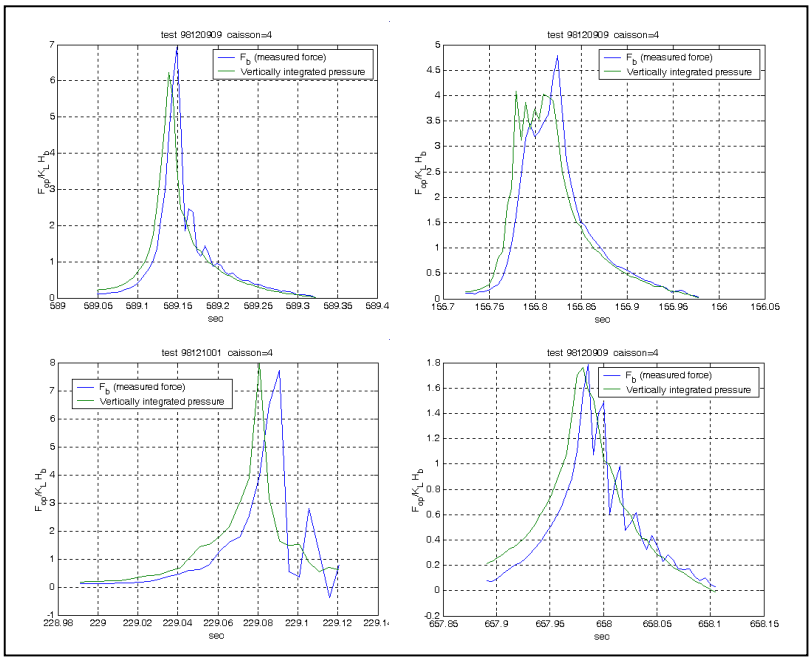

Figure 13. Impulsive forces and pressures on a caisson breakwater (after Martinelli & Lamberti, 2002).

Severe local damage, fatigue failure and local yielding may be caused by dynamic impact forces acting on small areas for a short duration. Available evidence shows that impact forces vary substantially in both magnitude and duration, differing significantly under nominally identical conditions. Laboratory studies show that air entrapment and entrainment are important in determining pressure/force maxima and this mechanism is mainly responsible for the scale effects.

After the initial contact between the wave and the element, the wave "travels" through the element, transferring a quasi-static force due to the mass of water. It is widely recognised that the main pulsating wave effects scale with Froude without the need for any significant correction.

Impulsive events necessarily involve compression over short durations of air entrained into the wave, which has the effect of a reduction of impact pressures (forces). This process does not scale neither by Froude nor by Cauchy, with different phases of the compression/expansion processes scaling differently (Allsop *et al.,* 1996; Howarth *et al.,* 1996). The problem is compounded by different values of air content between model and prototype, and between fresh and sea water. At model scale, the compressibility of water is reduced with respect to prototype in absolute and relative terms. This leads to sharper impact pressure signals with shorter rise time and larger magnitude at model scale if Froude law is applied for scaling. Wave impact studies on rubble mound armour units suggest that impulsive wave forces from small scale tests may be over-estimated by approximately a factor of 2 by using Froude scaling (Allsop *et al.,* 1995 and 1996; Howarth *et al.,* 1996), but those early studies do not give wider guidance. Analysis by Oumeraci *et al.* (1999 and 2001) shows that the processes of scale correction are complex, and that guidance to improve the reliability of design methods could be obtained by further controlled testing at large scale. The over-estimation of impulsive events obtained if using Froude law to scale model data, results from a combination of factors:

- air content in sea water at prototype scale is significantly higher than in fresh water at model scale, see Section 5;
- compression of air in the air/water mixture, particularly at prototype scale, is a highly non linear process controlled by one main parameter, the environmental pressure, that does not scale down in model, see Section 5.4;
- model structures are stiffer than prototype. In general, this is rarely taken into account and little attention is paid to properly reducing material and structural stiffness when designing model structures, see Section 6.3.

6.2 Run-up and overtopping

In a Froude model there are scale effects associated to viscous forces and surface tension. OPTICREST (De Rouck *et al.*, 2001) project showed that run-up was underestimated in normal small scale models; therefore, it is expected to be the same in the case of overtopping. Kajima & Sakakiyama (1994) confirmed that this is the case and stated that Re_c was similar to that for armour stability (i.e. $Re_c = 4 \cdot 10^5$). This will be further investigated in the EU-project CLASH. However, scale effects on overtopping are noticeable probably only for very small overtopping discharges (Schüttrumpf, 2001), but it is expected to be marginal for low crested structures where overtopping discharge is large. Initial analysis of a recent set of experiments on wave overtopping at large and small scales (University of Edinburgh-Sheffield) suggests that bulk overtopping flows scale directly by Froude without need for any significant correction (Pearson *et al.,* 2002).

6.3 Structure Deformation

An effect similar to compressibility of air is associated to structure compliance, that can be due to element flexibility or to foundation compliance. A description of the first effects can be found in Hattori *et al.* (1994) and Tirindelli *et al.* (2002a), of the second effect in Oumeraci *et al.* (2001) and Martinelli & Lamberti (2002).

6.4 Porous flow

There is a significant scale effect if the type of flow is different from a scale model to the corresponding flow in prototype. Typically, in a Froude small scale model the flow in the core material will be almost entirely laminar, whereas in the prototype core the flow will be turbulent at least in a considerable part of the core. A complete correction for this scale effect cannot be obtained just by further increasing the size (diameter) of the core material in the model with respect to the one given by the model length scale, because Reynolds number varies in time and space under the action of waves. Some fundamental publications on wave induced porous flow are Biésel (1950), Le Méhauté (1957, 1958), Jensen and Klinting (1983), Bürger *et al.* (1988), and Burcharth *et al.* (1999). The latter contains a practical engineering method for the scaling of the core material in conventional rubble mound breakwaters. The method involves determination of a characteristic flow velocity describing the interior velocity field.

6.5 Flow forces on plants and organisms

Forces on organisms attached to the surface of the breakwater armour are very difficult to scale correctly in small scale models because Reynolds number will often be in a range where the drag coefficients vary considerably (but see Denny, 1995). It is recommended that studies should be performed in the field under prototype conditions.

7. Movale-Bed Scale Effects

7.1 Generalities

When addressing the issue of scale effects for movable beds, major problems arise because of the need of modelling hydrodynamic as well as sediment parameters. Scale effects in movable bed models are not as well understood as those in fixed bed models, which have been described in the previous sections. The interaction between hydrodynamic forces and sediment eventually causes the motion of bed particles, which generates sediment transport patterns.

There are two approaches to determining important parameters (and resulting scaling relationships) for the coastal sediment transport model: a) assuming that sediment is primarly moved by currents; b) assuming that sediment is reacting primarly to waves. Kamphuis (1985) pointed out that waves move most of the sediment in a coastal model; this approach (waves model with currents added) is adopted in this section.

Sediment is transported as bed load or suspended load or possibly both. The dominant mode of transport in the prototype should be maintained in the model. In situations were both modes of transport occur (i.e. in situations involving cross-shore and long-shore transport (Kraus & McDougal, 1996)), but neither is dominant, only qualitative results can be obtained as it is not possible to scale bed load and suspended load simultaneously.

Grains remain in suspension in cases where the upward turbulent component of velocity (which is related to the skin friction shear velocity) exceeds the grain settling velocity (w_s). Therefore, sediment grains will remain in suspension as long as the relative fall speed (u_*/w_s) is greater than one. The scaling choice will depend on whether the flow is wave or current dominated.

The total bed shear stress (τ_b) acting on the bed is made up of contributions from: skin friction, which acts upon the grains and causes movement; form drag, caused by the pressure field due to flow over bedforms (e.g. ripples); sediment transport, resulting from the momentum transfer of the moving sediment grains. Therefore, it is important to be aware of how these various components of shear stress vary with changes in the bed profile and amount of sediment in suspension.

The following issues are mostly derived from Hughes (1993).

7.2 Hydrodynamic and sediment parameters

The important physical parameters involved in coastal sediment transport have been identified, see Table 3.

H	Wave height	Hydrodynamic
T	Wave period	Hydrodynamic
L	Wavelength	Hydrodynamic
λ	Characteristic length	Hydrodynamic
x, y, z	Coordinates	Hydrodynamic
t	time	Hydrodynamic
h	Local water depth	Hydrodynamic
g	gravity	Hydrodynamic
k_s	Bottom roughness	Hydrodynamic
ρ	Water density	Hydrodynamic
ν	Water kinematic viscosity	Hydrodynamic
D	Sediment diameter	Sediment
ρ_s	Sediment density	Sediment
τ_b	Bottom shear stress	Sediment
w_s	Sediment fall speed	Sediment

Table 3. Physical parameters in movable beds model

Parameters listed in Table 3 can be re-arranged as dimensionless.

The hydrodynamic set can be expressed as:

$$\Pi_H = f\left[\frac{H}{L}, \frac{h}{L}, \frac{x}{L}, \frac{y}{L}, \frac{z}{L}, \frac{k_s}{L}, t\sqrt{\frac{g}{L}}, \frac{\nu}{L\sqrt{gL}}\right] \tag{28}$$

The hydrodynamic phase of dimensionless parameters can be scaled using Froude law, admitting that some scale effects due to viscous effects and prototype-scale bedforms may be present.

Combining together parameters of Table 3, two sets of dimensionless parameters (the first one is from Kamphuis, 1991; the second one from Dalrymple, 1989) are derived.

$$\Pi'_{S_0} = g'\left[\frac{u_* d}{\nu}, \frac{\rho u_*^2}{\gamma_i d}, \frac{\rho_s}{\rho}, \frac{\lambda}{d}, \frac{w_s}{v_*}\right] \tag{29}$$

$$\Pi_S = g\left[\frac{u_* d}{\nu}, \frac{\rho u_*^2}{\gamma_i d}, \frac{\rho_s}{\rho}, \frac{H}{wT}\right] \tag{30}$$

where $u_* = (\tau_b/\rho)^{0.5}$, $\gamma_i = g(\rho_s-\rho)$.

Kamphuis (1991) also derived another set of parameters for breaking conditions.

$$\Pi_{Sb} = g'\left[\frac{\sqrt{gH_b}\,d}{\nu}, \frac{\rho g H_b}{\gamma_i d}, \frac{\rho_s}{\rho}, \frac{H_b}{d}, \frac{w_s}{\sqrt{gH_b}}\right] \tag{31}$$

Dimensionless number of equations 29-31 should be the same in the model and in the prototype. The main numbers are briefly reviewed below.

- *Densimetric Froude Number*

$$\frac{\rho u_*^2}{\gamma_i d} \tag{32}$$

- *Grain Reynolds Number* (relates the boundary roughness and the thickness of the viscous sub layer associated with the flow).

$$Re = \frac{u_* D}{\nu} \tag{33}$$

- *Dimensionless Grain Number*

$$D_* = \left[\frac{(\rho_S - \rho) g}{(\rho \nu^2)} \right]^{1/3} D \tag{34}$$

- *Shields Entrainment Parameter* (relates the applied bed shear stress to the immersed weight of the grains)

$$\vartheta = \frac{\tau_b}{(\rho_S - \rho) g} \tag{35}$$

Shields entrainment parameter (or in alternative densimetric Froude number) together with grain Reynolds number (or dimensionless grain number) can be used to determine whether the sediment will be set in motion (Miller *et al.*, 1977; Soulsby, 1997; Paphitis, 2001), se Figure 14, and, hence, must be scaled correctly otherwise the transport rate will be incorrect.

Shields parameter can be used also to determine the formation of bedforms. Soulsby (1997) provided a set of conditions for sediment mobility: a) $\theta < \theta_{cr}$ – then the bed is immobile; b) $\theta_{cr} < \theta < 0.8$ – then the bed is mobile and rippled; c) $\theta_{cr} > 0.8$ – then the bed is mobile and flat with sheet flow.

- *Dean Number* (an alternative fall speed parameter)

$$Dn = \frac{H}{w_s T} \tag{36}$$

As a general remark, not all parameters are independent and not all refer to the same process or relate to the same scale.

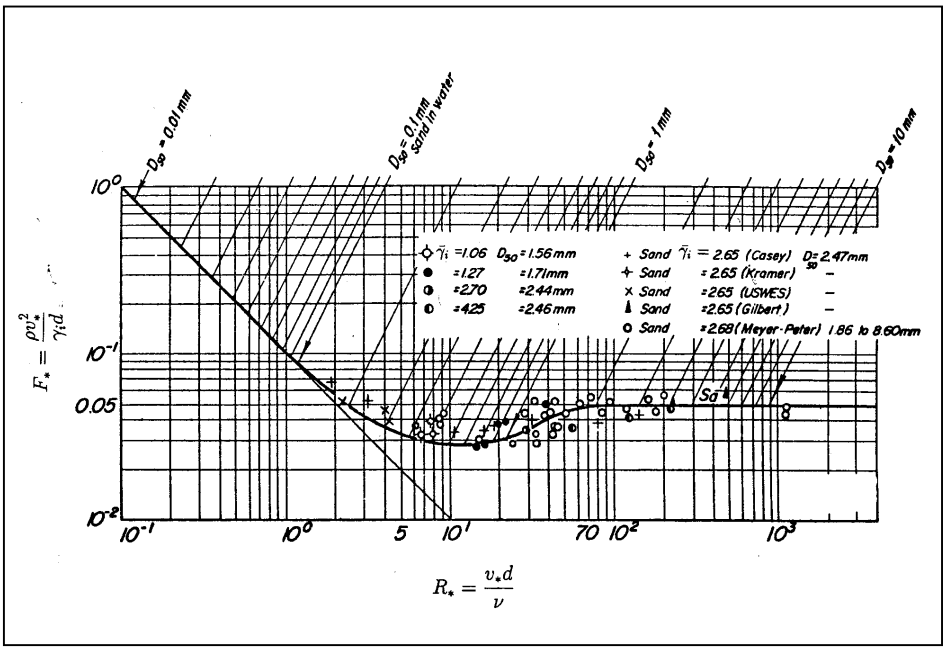

Figure 14. Shields diagram, after Hughes (1993)

As already pointed out, the main difference in sediment transport models depends whether bed or suspension load is the dominant mode of transport.

7.3 Bedload-dominated transport models

Perfect similitude could be obtained if all the parameters of Equation 29 are maintained from prototype to model. This is impossible, some scale effects are necessarily to be accounted for. Table 4 shows a review by Kamphuis (1985) of several similitudes in which some of the parameters are preserved from prototype to model.

Model Class	$\frac{v_* d}{\nu}$	$\frac{\rho v_*^2}{\gamma_i d}$	$\frac{\rho_s}{\rho}$	$\frac{\lambda}{d}$	$\frac{\omega}{v_*}$
Best Model (BM)	o	•	•	•	o
Lightweight Model (LWM)	•	•	o_1	o	o
Densimetric Froude Model (DFM)	o	•	o_1	o	o
Sand Model (SM)	o	o	•	o	o

• Satisfied
o Not Satisfied
o_1 Not satisfied but limited to $1.05 < \rho_s/\rho < 2.65$

Table 4. Classification of coastal models (after Kamphuis, 1985)

From Table 4, it can be pointed out that the first model (Best Model) is the one that satisfies the higher number of sediment transport criteria, hence the name. Its main limitations consist in the following:

- The requirement that model sediment be reduced as model length scale, see Section 7.5.
- Reynolds number is not maintained ⇒ it is necessary to work in an environment where viscous forces are small (i.e. turbulent regime).
- The ratio between fall and shear velocity is reduced in model: this is not a major problem when bedload is considered, it may affect suspended transport.
- Distortion in roughness due to eventual bedforms.

7.4 Suspended load-dominated transport models

Suspended mode of transport depends on a different set of parameters than bedload transport. Sediment are suspended from the bed and transported by currents if a considerable state of turbulence is present in the field. This generally happens in the breaking zone, so Equation 31 can be used for this type of transport.

The main dimensionless parameter involved in suspended transport can be identified as the dimensionless fall speed parameter or the Dean Number, already seen in Equation 36. This parameter can be seen as the ratio between H/ws (the time taken for a sand particle to fall a distance equal to wave height) and the wave period T. If Dn is lower than 1, the main transport will be bedload, suspension will therefore dominate when Dn > 1.

The main scale effects for this type of transport arise from the fact that Shields Parameter is not preserved. High levels of turbulence are however responsible for mobilisation of sediment in the surf zone, therefore this scale effect is thought to be not so relevant. The use of lightweight sediment to overcome the problem of having too fine model particles is sometime encouraged, but can induce further scale effects due to different accelerations of particles from prototype to model.

7.5 Scour at the trunk section

An interesting overview of scour processes at the trunk of a breakwater is given by Sumer & Fredsoe (2002). They list the dimensionless parameters responsible for scour as:

$$\frac{S}{H} = f\left[\frac{h}{L}, \alpha, \theta, \frac{L}{d}, \mathrm{Re}\right] \tag{37}$$

where α is slope of the breakwater and θ is incident wave direction.

The same kind of law can be defined for the time scale of scour:

$$T^* = T^*\left[\frac{h}{L}, \alpha, \theta, \frac{L}{d}, \mathrm{Re}\right] \tag{38}$$

where:

$$T^* = \frac{\left(g \cdot (s-1) \cdot d^3\right)^{\frac{1}{2}}}{H^2} \cdot T \tag{39}$$

where s is the specific gravity for sand grains.

7.6 Overview on scale effects on sediment transport

As anticipated, the various dimensionless parameters, which incorporate the grain size (*D*) cannot be modelled correctly. The inability to scale down grain size correctly results in the most pronounced scale effects in mobile bed models. The main problem is due to the fact that if selected scaling criteria require that grain size be scaled the same as geometric length scale, the presence of very fine (< 0.08mm) sediment might appear in the model, giving rise to non-cohesive sediment, therefore not respecting sediment characteristics of the prototype. This might be overcome by using model sediment having different sizes and different density than prototype.

A complete understanding of all scale effects is very difficult given the incomplete theoretical background of the sediment transport mechanisms which involve sediment suspension, liquefaction of the bed, percolation and aeration of the breaker zone.

Inertial effects relate to the mobile sediment and whether that is moving in suspension or bed load; the importance of this was highlighted previously. Sawaragi and Deguchi (1978) suggested criteria based on the dimensionless parameter *H/D* (where *H* is the wave height) to distinguish between prominence of bed load versus suspended load, such as:

- If $H/D < 125$ – bed load;
- If $200 < H/D < 300$ – sediment is suspended (transition);
- If $H/D > 300$ – suspended load exceeds bed load.

Therefore, the dominant transport mechanism in the prototype will drive the selection of the model grain size in order to ensure and being able to induce suspended load or bed load sediment movement.

Viscosity effects complicate scaling exercises in several ways. It is often assumed that the effects of viscosity are negligible due to the high turbulence induced around structures, but flow reversals under waves give rise to smooth flow regimes in the boundary layer, especially outside the breaker zone. Outside the near-field zone of the structures the flow will undergo through the transition from laminar to turbulent flow in the boundary layer. In this region an increase in grain size intensifies turbulence which, in turn, induces greater sediment mobility. Beyond 0.6mm (Komar and Miller, 1974; Madsen and Grant, 1976; Kamphuis and Nairn, 1984) the boundary layer flow is fully developed rough turbulent and any further increases in grain diameter do not result in proportional increases in sediment mobility; this phenomenon stands for both unidirectional and oscillatory fluid motion.

As a final, general comment, sediment is not scaled the same as geometry or hydrodynamics. Moreover, care must be taken when in presence of bedforms, which scale differently in mobile bed tests depending on geometric scale and also on the dominant process.

8. Effects of Marine Growth on Rubble Mound Breakwaters

Various organisms attach to hard substrate ranging from microbial films, thin layers of filamentous algae, thin sheets of barnacles, dense beds of mussels, thick algal turfs, and large leathery seaweeds such as fucoids and kelps. The composition and, hence, thickness of marine growth depends on a variety of biotic and abiotic factors.

8.1 Biological and physical factors affecting marine growth

Biological limits to marine growth include local larval supply, nutrients and food availability (Denny, 1988). Rates of growth, coverage and thickness of marine growth can also be strongly reduced by biological interactions such as molluscs and sea urchin grazing, starfish and crab predation. Thickness of growth will generally increase with time, but may reach a maximum at an intermediate stage, in presence of predation.

Bio-geographic location, water depth, wave action, disturbance regime (scouring, inundation etc.), have an important influence on the rate growth of marine organisms. On wave-swept shores, hydrodynamic forces from breaking waves are thought to limit the size of plants and animals because of the increased risk of dislodgment or damage. Denny (1999) suggested that the combination of drag and water acceleration is likely to control the maximum size of wave swept organisms, although hard bodied invertebrate, which are more firmly attached to the substratum, appeared to be less affected by these hydrodynamic forces.

8.2 Effects of marine growth on hydrodynamics of rubble mound breakwaters

It is known that marine organisms attached to off-shore platforms increase considerably the surface roughness and the member diameter, thus increase drag and inertia loads around the structure (Heideman & George, 1981). On wave swept shores, the presence of organisms such as limpets, mussels and barnacles generally increase drag forces (Denny, 1989; Denny, 1995; Denny *et al.*, 1998). Similarly, the epibiota colonising rubble mound structures can have serious consequences on the local hydrodynamics. These organisms can also colonise the pores causing reduction in the water flow through the structure. In addition, the diameter of the pore can be further reduced by large quantity of sediment which is often trapped in algal turfs and mussel beds.

Scarce information on thickness of marine growth is available from literature. This is mainly related to studies on marine fouling on man-made off-shore structures, where marine growth is monitored at depths greater than 10 m (Forteath *et al.*, 1982; Yan *et al.*, 2000). In such systems, thickness of fouling is up to 8 cm while growth tends to stabilise after 35 months (Mitra, 1991; Heideman & George, 1981). Maximum values of growth of algae and marine invertebrates commonly found on rocky shores in UK are listed in Table 5.

Species	Max. size (cm)
Green Algae	
Enteromorpha spp.	75
Cladophora rupestris	12
Ulva lactuca	20
Ectocarpus sp.	30
Brown algae (fucoids)	
Pelvetia canaliculata	15
Fucus spiralis	40
Fucus vesiculosus	100
Fucus serratus	60
Ascophyllum nodosum	>100
Brown algae (kelps)	
Laminaria digitata	200
Laminaria hyperborea	350
Laminaria saccharina	400
Sacchoriza polyschides	450

Species	Max. size (cm)
Red Algae	
Chondrus crispus	15
Mastocarpus stellatus	17
Corallina officinalis	12
Lithothamnia	2
Lomentaria articulata	10
Palmaria palmata	30
Laurencia pinnatifida	20
Porphyra spp.	60
Ceramium spp.	30
Molluscs	
Patella vulgata	6
Patella depressa	3
Ostrea edulis	10
Mytilus edulis	20

Table 5. Maximum values of growth of intertidal and subtidal species. Values given for algae refer to maximum length of fronds; Values given for molluscs refer to maximum shell length.

Also the effects of bio-turbation on sediment transport and the resulting morphodynamics should be considered, when necessary.

8.3 An experimental evaluation of marine growth on breakwaters in UK

As part of research carried out in DELOS, field data were collected in July-August 2002 to assess thickness of marine growth on LCS and consequent reduction of the pore size. The study was carried out in Liverpool (Merseyside) on four LCS. Thickness of marine growth was measured in approximately 15 pores of different size on each structure. Results are given in Table 6.

	Pore diameter (cm)	**Thickness of marine growth (cm)**		**Reduction in pore size (%)**	
	Mean value	Mean value	Max. value	Mean value	Max. value
Fucoids	65.4 (4.26)	2.1 (0.29)	3.8	6.6 (0.91)	12.6
Mussels	44.4 (2.32)	6.7 (0.91)	15.8	31.1 (4.41)	78.8
Barnacles	57.1 (4.94)	0.7 (0.06)	1	2.6 (0.35)	6.7

Table 6. Pore size (given as approximate pore diameter), maximum and mean values of thickness of algae and marine invertebrates around the pores and percentage of reduction of the pore size due to the presence of marine growth. Results are given for selected pores where fucoids, mussels or barnacles were dominant (>60% cover). Values in brackets refer to standard error.

Mussel cover around the pores was up to 16 cm thick. Some of the pores were completely filled up with several strata of mussels and the pore size was reduced more then 70%. Brown algae and barnacles appeared not to have such effect, as thickness usually was not greater than 4 cm. Moreover, the effect of marine growth resulting in the reduction of the pore size appeared to be slightly dependent on the actual diameter of the pore. The reduction in pore

diameter due to the presence of attached organisms was less evident in bigger pores (>60 cm diameter), as shown in Figure. 15.

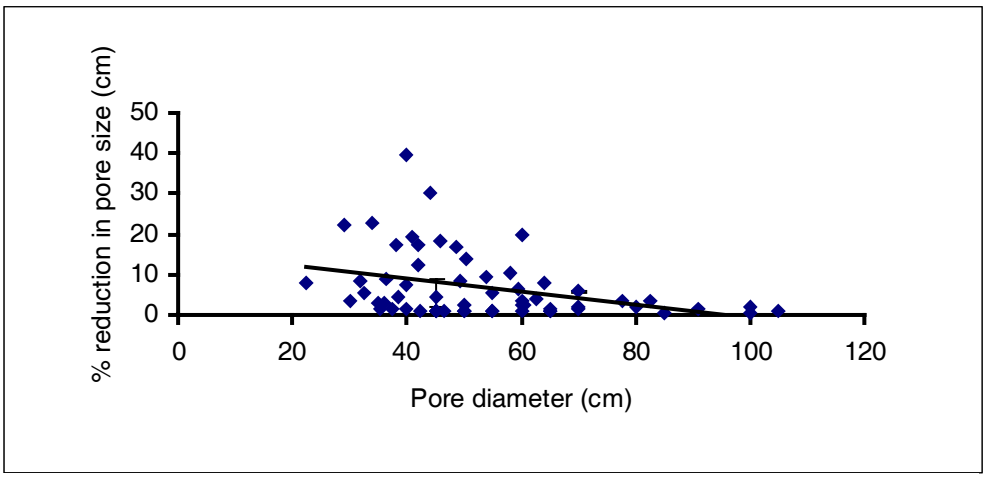

Figure 15. Relation between pore diameter and percentage of reduction of pores due to marine growth (R^2=0.1309, P<0.01)

9. Conclusions

This report summarises the problem of scale effects for physical modelling on wave-induced impacts on rubble mound breakwaters. The main points to be taken in account when transferring model results to prototype dimensions can be summarised as follows.

1) None of the standard scaling laws for hydraulic models (Froude, Cauchy, Reynolds, Weber) provides accurate scaling for all processes of wave-related breakwater models. Scale effects from prototype to model are due to: intrinsic properties of breakers (surface tension, air content); wave-structure interactions; different ambient conditions in field and laboratory (sediment scaling and effects of algae and mussels).

2) The main scale effects in wave-structure interactions can be listed as: wave impacts on armour blocks; run-up and overtopping; structure deformation; wave generated flow in the porous structure; flow forces on plants and organisms attached to the structure

3) Impact wave loads on mound breakwaters are compounded of two parts: impulsive load (sharp peak, high magnitude, short rise time); pulsating (quasi-static) load associated to the mass of water "travelling" through the structure.

   - No major scale effects are evident when dealing with pulsating loads. In this case Froude scaling is accurate enough to transfer model results to prototype scale.
   - Impulsive loads induced by breaking waves involve compressibility of air during a very short time. The fluid interacting with the structure becomes a mixture air/water and can not be treated as an incompressible fluid. Froude law is therefore not adequate for scaling model results on impulsive events. The application of Cauchy law to the whole process has proved to be inaccurate as well. Surface tension can dramatically alter the deformation of the crest shape as the approaching waves break.

4) Surface tension effects become increasingly important as the wavelength and intensity of the breaker decreases. Without surface tension the crest deforms to generate a jet (or

perhaps a three-dimensional jet-like structure) at the crest that plunges into the wave face to start the turbulent spilling process. When surface tension effects become dominant, this jet is replaced by a bulge-capillary structure at the crest and turbulence is produced by separation at the point of high-upward surface curvature (toe) at the leading edge of the bulge.

5) During the turbulent spilling process, for cases where surface tension is unimportant, dramatic splashing motions occur, and air bubbles and water droplets are produced. When surface tension is dominant, the surface fluctuations (and perhaps turbulence) are reduced, and a single continuous bumpy surface makes up the boundary between air and water. Theoretical and experimental investigations have emphasized the importance of the shear layer between the fluid in the leading edge of the breaking region and the fast-moving underlying flow as the sit of strong turbulence generation.

6) Because in the natural world surfactants are nearly always present, their effect on spilling breakers should be investigated. Surfactants will have strong effects on surface-tension-dominated breakers.

7) The different compressibility of water is due to the different process of bubble formation from fresh water (used in physical models) to sea water. Typical air bubbles are smaller in sea water than in fresh water and have the tendency to remain entrained in a breaking wave. Furthermore, their size distribution is also different from fresh to sea water.

8) The factors causing the differences in bubble sizes and distribution between prototype sea water and model fresh water can be listed as: salt concentration, ionic structure, exudates of marine organisms, surface tension, temperature and viscosity.

9) The main effects of the different compressibility of water from model to prototype is in an overestimation of pressure magnitude and underestimation of pressure rise time for impulsive loading, if Froude or Cauchy laws are used for transferring model to prototype results. This happens because in aerated water (sea water), the presence of air produces a “cushioning” effect, which weakens the magnitude of the impact and extends its duration.

10) Considering that inertia forces scale as U^2, also a straightforward use of Weber law would lead to errors, given that $We = \frac{\rho U^2 l}{\sigma}$, and that surface tension does not scale from model to prototype.

11) It is suggested to analyse wave loading by use of the parameter impulse: $\int \mathrm{p(t)}\, dt$, i.e. the integral of pressure or force over time during the impulsive event. Scaling model impulses to prototype dimensions by use of Froude law generally gives accurate results even for highly impulsive events.

12) Another parameter which can be used for impulsive events analysis is $\int \frac{dp}{\rho}$. This parameter is a function of percentage void ratio. Therefore, the use of this parameter involves the need for accurate measurements of air content in model and prototype scales.

13) Even when comparing model tests carried out with sea water to full scale field results, differences can be noted in the maximum impulsive pressures. The different environments (laboratory and field) play a decisive role and affect the ambient conditions of the experiment.

14) Run-up seems to be influenced by scale effects, even though not many quantitative data are available. Overtopping seems to scale down accurately by use of Froude law, even though for small values of discharge some scale effects might cause underestimation in small scale models.

15) Porous flow in model is almost entirely laminar, whereas in field condition the motion is turbulent. Some empirical engineering methods exist for scale corrections.

16) Forces on plants and organisms should be directly measured in field conditions, as model tests are highly influenced by complex scale effects.

17) In relation to sediment scaling the transport mode in the prototype should be maintained in the model. The parameter which is used to asses which kind of transport is dominating (bedload or suspended transport) is Dean parameter $Dn = \frac{H}{w_s T}$.

18) In situations were both modes of transport (suspension – no suspension) occur, only qualitative results can be obtained as it is not possible to scale bed load and suspended load simultaneously.

19) A correct scaling for sediment preserves Dean parameter, uses an undistorted geometrical scale and scales hydrodynamics through Froude law. A model like this preserves similarity in wave form, sediment fall path, wave-induced velocities, break point, breaker type, wave decay (provided the model is large enough to minimise viscous and surface tension effects). Important scale effects however arise when the viscous domain becomes dominant and in presence of ripples.

20) Marine organisms attached to breakwaters increase structure roughness, reduce the water flow through the structure and can trap large quantity of sediment. The combination of these effects significantly affects flow through the structure. Therefore care must be taken when scaling from field to model condition, in order to correctly evaluate these effects.

Selected References

Adamsom, A.W. (1990) "Physical Chemistry of Surfaces" John Whiley & Sons, Inc. 777

Allsop N.W.H., Vicinanza D., & McKenna J.E. (1996) "Wave forces on vertical and composite breakwaters" Strategic Research Report SR 443, pp 1-94, HR Wallingford, March 1996, Wallingford

Allsop N.W.H., Vann A.M., Howarth M., Jones R.J. & Davis J.P. (1995) "Measurements of wave impacts at full scale: results of fieldwork on concrete armour units" pp287-302, Conf. on Coastal Structures and Breakwaters '95, ICE, ISBN 0 7277 2509 2, publn. Thomas Telford, London

Apel J.R. (1987). "Principles of Ocean Physics" International Geophysics Series, Vol. 38, Academic Press, Orlando.

Biésel F. (1950) "Equations de l'écoulement non lent en milieu permeable" La Houille Blanche, No. 2.

Bonmarin, P.J. (1989) "Geometric properties of deep-water breaking waves" Journal of Fluid Mechanics, 209: 405-433

Broderick L.L. & Ahrens J.P (1982) "Riprap stability scale effects" CERC technical paper No. 82-3, U.S.A.

Bullock G.N., Crawford A., Hewson P., Walkden M.J.A. & Bird. P.A.D. (2001) "The influence of air and scale on wave impact pressures" Coastal Engineering, 42, 4, 291-312

Burcharth H.F., Liu Z. & Troch P. (1999) "Scaling of core material in rubble mound breakwater model tests" Proc. 5th COPEDEC, Cape Town, South Africa, pp. 1518-1528.

Bürger W., Oumeraci H. & Partenscky H.W. (1988) "Geohydraulic investigations of rubble mound breakwaters" Proc. 21th ICCE, Malaga, Spain.

Cartmill J. & Su M-Y. (1993) "Bubble Size Distribution Under Saltwater and Freshwater Breaking Waves" Dynamics of Atmos. And Ocean. 20: 25-31

Ceniceros H.D. & Hou T.Y. (1999) "Dynamic generation of capillary waves" Phys. Fluids 11(5): 1042-1050

Chanson H., Aoki S. & Hoque A. (2002) "Similitude of Air Bubble entrainment and Dispersion in Vertical Circular Plunging Jet Flows. An Experimental Study with Fresh water, Salty Fresh water and Sea water". Coastal/Ocean Engineering Report, No. COE02-1, Dept. of Architecture and Civil Engineering, Toyohashi University of Technology, Japan, 2002-04-04

Craig V.S.G, Ninham B.W. & Pashley R.M. (1993) "Effect of electrolytes on bubble coalescence" Nature, 364, 317-319

Cruickshank I. & Allsop N.W.H. (2001) "Guidelines for the hydraulic design of exposed jetties" Interim report n°2 SR Report 583 DTI PII Project 39/5/130 cc2035, HR Wallingford

Dai Y.B. & Kamel,A.M. (1969) "Scale effect tests for rubble mound breakwaters" U.S. Army Engineer Waterway Experiment Station, Cops og Engineers, Vicksburg, Mississippi, Research Report H-69-2.

Dalrlymple R.A. (1989) "Physical Modelling of Littoral Processes", in Recent Advances in Hydraulic Physical Modelling", R. Martins, Ed., Kluwer Academic Publishers, Dordrecht, The Netherlands, pp 567-588

Datta R., Napier D.H. & Newitt D.M. (1950); Trans. Inst. Chem. Engrs, London, vol.28, 14. Quoted in Lane W.R. & Green H.L. (1956), The mechanics of drops and bubbles. In Surveys in mechanics, Batchelor G.K. & Davies R.M. ed., Cambridge Univ. Press, 162-215.

Denny M. (1988) "Biology and the mechanics of the wave-swept environment" Priceton, NJ: Princeton University Press.

Denny M. (1989) "A limpet shell shape that reduces drag: a laboratory demonstration of a hydrodynamic mechanism, and an exploration of its effectiveness in nature" Canadian Journal of Zoology, 67: 2098-2106.

De Rouck J., Boone C. & Van de Walle B. (2001) "The optimisation of crest level design of sloping coastal structures through prototype monitoring and modelling" Final Report EU-MAST III OPTICREST project. University of Ghent, Belgium.

Del Grosso V.A., (1974) "New equation for the speed of sound in natural waters (with comparison to other equation)" J. Acoustic. Soc. Amer., 83, 2180-2185.

Denny M. (1995) "Predicting physical disturbance: mechanistic approaches to the study of survivorship on wave-swept shores" Ecological Monographs, 65 (4): 371-418.

Denny M., Gaylord B., Helmuth B. & Daniel T. (1988) "The menace of momentum: dynamic forces on flexible organisms" Limnology and Oceanography, 43 (5): 955-968.

Dimas A.A. (1997) "Large wave simulations (LWS) of free-surface flows" ASME Fluids Eng. Summer Meet. Vancouver, Can. June 22-26, FEDSM97-3408, pp. 1-6.

Dimas A.A. & Fialkowski L-T. (2000) "Large-wave simulation (LWS) of free-surface flows developing weak spilling breaking waves" J. Comput. Phys. 159(2):172-196.

Dold, J.W & Peregrine, D.H. (1986) "Water-wave modulation" Proc. 20th Conf. Coastal Engineering, ASCE, 1: 163-175.

Donelan, M., Longuet.Higgins, M.S. & Turner, J.S. (1972) "Periodicity in whitecaps" Nature, 239: 449-451.

Duncan J.H, Philomin V., Behres M. & Kimmel J. (1994a). "The formation of spilling breaking water waves" Phys. Fluids, 6: 2558-2560.

Duncan J.H, Philomin V., Qiao H., Kimmel J. (1994b) "The formation of a spilling breaker" Phys. Fluids 6: S2.

Duncan J.H, Qiao H., Philomin V. & Wienz A. (1999) "Gentle spilling breaker: crest profile evolution" Journal of Fluid Mechanics, 379: 191:222.

Duncan J.H. (2000) "Spilling breakers" Ann. Rev. Fluid Mechanics. 33: 519-547.

Dushaw B.D., Worcester P.E., Cornuelle B.D. & Howe B.M. (1993) "On equations for the speed of sound in sea water" J. Acoustic. Soc. Amer., 93, 255-275.

Etter P.C. (1996) "Underwater Acoustic Modeling: Principles, Techniques and Applications" 2nd Ed., E & FN Spon, London.

Forteath G. N. R., Picken G. B., Ralph R. & Willimas J. (1982) "Marine growth studies on the North Sea Oil Platform Montrose Alpha" Marine Ecology Progress Series, 8: 61-68.

Frye H.W. & Pugh J.D. (1971) "A new equation for the speed of sound in sea water" J. Acoustic. Soc. Amer., 50, 384-386.

Haines M.A. & Johnson B.D. (1995) "Injected bubble populations in sea water and fresh water measured by a photographic method" Journal of Geophysical Research, 100, 70567-7068.

Hamilton, E.L., 1980. Geoacoustic modeling of the sea floor. J. Acoustic. Soc. Amer., 68, 1313-1340.

Hattori M., A. Arami & T. Yui (1994). "Wave impact pressure on vertical walls under breaking waves of various types", Coastal Engineering, 22, 79-114

Heideman J.C. & George R.J. (1981) "Biological and engineering parameters for macrofouling growth on platforms offshore Lousiana" The Ocean – An international workplace. Oceans 81 Conference Record – Boston, Massachussets, September 16-18, 1981, vol. 1: 550-557.

Hitachi S. (1994) "Case study of breakwater damages Mutsu-Ogawara Port" Proc. Int. Workshop on Wave Barriers in Deepwaters, Port and Harbours Research Institute, Yokosuka, Japan, 308-331.

Howarth M.W., Allsop N.W.H., Vann A.M., Davis J.P., & Jones R.J. (1996) "Scale effects of wave impact pressures on cob armour units" Proceedings of 25th International Conference on Coastal Engineering, Orlando, Florida, September 2-6, 2522-2531, Ed Billy L Edge, published by American Society of Civil Engineers, New York.

Hughes S.A. (1993) "Physical models and laboratory techniques in coastal engineering" World Scientific Publishing Co, Singapore.

Jensen O.J. & Klinting P. (1983) "Evaluation of scale effects in hydraulic models by analysis of laminar and turbulent flows" Coastal Engineering, 7, 319-329.

Kajima R. & Sakakiyama T. (1994) "Review of works using CRIEPI flume and present work" Proc. Coastal Dynamics, Barcelona, Spain, pp. 614-627.

Kamphuis J.W. (1991) "Physical Modeling", in Handbook of Coastal and Ocean Engineering", J.B. Herbich, Ed., Vol. 2, Gulf Publishing Company, Houston, Texas

Kamphuis J.W. (1985) "On Understanding Scale Effect in Coastal Mobile Bed Models" Physical Modelling in Coastal Engineering, R. A. Dalrymple, Ed., A. A. Balkema, Rotterdam, The Netherlands, pp. 141-162

Kamphuis J.W. & Nairn R.D. (1984) "Scale effects in large coastal mobile bed models" Proceedings of the 19th International Conference on Coastal Engineering, Houston, 2322-2338.

Kinsler L.E., Frey A.R. Coppens A.B. & Sanders J.V. (1982) "Fundamentals of Acoustics" 3rd Ed., John Wiley and Sons, New York.

Komar P.D. & Miller M.C. (1974) "Sediment transport under oscillatory waves" Proceedings of the 14th International Conference on Coastal Engineering, Copenhagen, 756-775.

Kraus N.C. & McDougal W.G. (1996) "The effects of seawalls on the beach: part 1, an updated literature review" J. Coastal Res., 12(3), 691-701.

Le Méhauté B. (1957 and 1958) "Perméabilité des digues en enrochements aux ondes de graivté periodiques" La Houille Blanche No. 6, 1957 and No. 2, 3, 1958.

Leroy C.C. (1969) "Development of simple equations for accurate and more realistic calculation of the speed of sound in sea water" J. Acoustic. Soc. Amer., 46, 216-226.

Longuet-Higgins M.S. & Turner J.S. (1974) "An "entraining plume" model of a spilling breaker" Journal of Fluids Mechanics. 63: 1-20

Longuet-Higgins M.S. (1994) "Shear instability in spilling breakers" Proc. R. Soc. London. Ser: A 446:399-409

Longuet-Higgins M.S. & Cleaver R.P. (1994) "Crest instabilities of gravity waves. 1. The almost highest wave" Journal of Fluid Mechanics, 258: 115-129

Longuet-Higgins M.S., Cleaver, R.P. & Fox, M.J.H. (1994) "Crest instabilities of gravity waves.2. Matching and asymptotic analysis" Journal of Fluid Mechanics, 259: 333-344

Longuet-Higgins M.S. (1997) "Progress towards understanding how waves break" Symp. Nav. Hydrodyn. 21st, Trondheim, Nor. June 1996, pp.7-28

Longuet-Higgins M.S. & DommermuthD.G. (1997) "Crest instabilities of gravity waves. Part 3. Non-linear development and breaking" Journal of Fluid Mechanics. 336: 33-50

Mackenzie K.V. (1981) "Nine-term equation for sound speed in the oceans" J. Acoustic. Soc. Amer., 70, 807-812

Madsen O.S. & Grant W.D. (1976) "Quantitative description of sediment transport by waves" Proceedings of the 15th International Conference on Coastal Engineering, Honolulu, 1093-1112

Martinelli L. & Lamberti A. (2002) "Statistical Characterisation of Breaking Wave Forces Applied by a Caisson Breakwaters to its Foundation" Paper presented at 28th ICCE (ASCE), Cardiff

Melville, W.K. (1982). The instability and breaking of deep-water waves. Journal of Fluid Mechanics 115: 163-185.

Melville W.K. (1996). The role of surface-wave breaking in air-sea interaction. Ann. Rev. Fluid Mech. 28: 279-321.

Miller M.C., McCace I.N. & Komar P.D. (1977) "Threshold of sediment motion under unidirectional currents" Sedimentology, 24, 507-527.

Mitra S. (1991) "Marine growth on offshore structures in Indian offshore waters and removal strategy" Proceedings of the first International offshore and polar engineering conference, 1: 143-147.

Mol A., Ligteringen H., Groeneveld R.L. & Pita C.R.A.M. (1983) "West Breakwater-Sines. Study of armour stability" Proc. Specialty Conference on the Design Maintenance and Performance of Coastal Structures, ASCE, Arlington, Virginia, U.S.A.

Monahan EC & Zeitlow CR (1969) "Laboratory comparisons of fresh water and salt-water whitecaps" Journal of Geophysical Research, 74, 6961-6966

Nystuen J.A. (1986) "Rainfall measurements using underwater ambient noise" J. Acoustic. Soc. Amer., 79, 972-982

Orcutt J.A. (1988) "Ultralow- and very-low-frequency seismic and acoustic noise in the Pacific" J. Acoustic. Soc. Amer., 84 (Suppl. 1), S194 (abstract)

Oumeraci H, Allsop N.W.H., de Groot M.B., Crouch R.S & Vrijling J.K (1999) "Probabilistic Design Methods for Vertical Breakwaters (PROVERBS)" Proc. Coastal Structures'99, Santander, Spain, publn. Balkema, Rotterdam

Oumeraci H., Kortenhaus A., Allsop N.W.H., De Groot M.B., Crouch R.S., Vrijling J.K. & Voortman H.G. (2001) "Probabilistic Design Tools for Vertical Breakwaters" 392 pp, ISBN 90 580 248 8, publn. Balkema, Rotterdam

Oumeraci H. (1994) "Review and analysis of vertical breakwater failure - lessons learned" Coastal Engineering 22, 3-29

Paphitis D. (2001) "Sediment Movement Under Unidirectional Flows: An Assessment of Empirical Threshold Curves" Coast. Eng., 43, 227-245

Pearson J., Bruce T. & Allsop N.W.H. (2002) "Violent wave overtopping - measurements at large and small scale", Paper presented at 28th ICCE (ASCE), Cardiff

Peregrine D.H. & Thais L. (1996) "The effect of entrained air in violent water wave impacts" J. Fluid Mech., Vol.325, pp 377-397

Perlin M., He J.H. & Bernal L.P. (1996) "An experimental study of deep water plunging breakers" Phys. Fluids 8(9): 2365-2374

Perlin M & Schultz P. (2000) "Capillary effects on surface waves" Ann. Rev. Fluid. Mech, 32: 241-274

Pumphrey H.C. & Crum L.A. (1990) "Free oscillations of near-surface bubbles as a source of the underwater noise of rain" J. Acoustic. Soc. Amer., 87, 142-148

Rapp R.J. & Melville, W.K. (1990) "Laboratory measurements of deep-water breaking waves" Philos. Trans. R. Soc. London Ser. A 331: 735-800

Sawaragi, T. & Deguchi, I., 1978 "Distribution of sand transport rates across a surf zone" Proceedings of the 16th International Conference on Coastal Engineering, Hamburg, 1596-1613

Schüttrumph H. (2001) "Wellenüberlaufströmning be Seedeichen – experimentelle und theoretische untersuchungen" Fachbereich Bauingenieurwesen, Technischen Universität, LWI, Braunschweig, Germany, Heft 149. (In German)

Sharp J.J. & Khader M.H.A. (1984) "Scale effects in harbour models involving permeable rubble mound structures" Symposium on Scale Effects in Modelling Hydraulic Structures, Kobus, H. (ed.), Esslingen, Germany, pp 7.12-1 – 7.12-5

Shaw P.T., Watts D.R. & Rossby H.T. (1978) "On the estimation of oceanic wind speed and stress from ambient noise measurements" Deep-Sea Res., 25, 1225-1233

Slauenwhite D.E. & Johnson B.D. (1999) "Bubble shattering: Differences in bubble formation in fresh water and sea water" Journal of Geophysical Research-Oceans, 104(C2), 1999, pp. 3265 – 3275

Slauenwhite DE & Johnson BD (1996) "The effect of organic matter on bubble surface tension in fresh water and sea water" Journal of Geophysical Research, 101, 3769-3774

Soulsby R.L. (1997) "Dynamics of marine sands: a manual for practical applications" Thomas Telford Services Ltd., London, 249 pp.

Spiesberger J.L. & Metzger K. (1991) "A new algorithm for sound speed in sea water" J. Acoustic. Soc. Amer., 89, 2677-2688

Stokes, G.G. (1880) "Considerations relative to the greatest height of oscillatory irrotational waves which can be propagated without change of form" Math. Phys. Papers 1: 225-228

Su M-Y. & Wesson J.C. (2001) "Bubble Measurement Techniques and Bubble Dynamics in Coastal Shallow Water" Adv. In Coastal Engineering, 7, 77-124

Sumer & Fredsoe (2002) "The mechanics of scour in the marine environment", Advanced Series on Ocean Engineering – volume 17, World Scientific

Thompson D.M. & Shuttler R.M. (1975) "Riprap design for wind wave attack. A laboratory study in random waves" HR Wallingford, U.K., Report EX 707

Tulin M.P. (1996) "Breaking of ocean waves and downshifting" Waves and Nonlinear Processes in Hydrodynamics, ed. J. Grue, B Gjevik, J.E. Weber, pp. 177-190. Dordrecht, Neth.: Kluwer Acad

Tirindelli M., Cuomo G., Allsop N.W.H & McConnell K. (2002a) "Exposed Jetties: Inconsistencies and Gaps in Design Methods for Wave-Induced Forces" Paper presented at 28th ICCE (ASCE), Cardiff

Van der Meer, J.W., 1988 "Rock slopes and gravel beaches under wave attack" Doctoral thesis. Delft University of Technology

Walkden M.J.A., Hewson P., Bullock G.N. & Bird P.A.D. (1996) "Wave impulse pressure prediction for caisson design" Proceedings of 25th International Conference on Coastal Engineering, Orlando, Florida, September 2-6, Ed Billy L Edge, vol 3, pp2584-2597, published by American Society of Civil Engineers, New York

Wilson W.D. (1960) "Equation for the speed of sound in sea water" J. Acoustic. Soc. Amer., 32, 1357

Yan T., Yan W., Liang G., Dong Y., Wang H. & Yan Y. (2000) "Marine biofouling in offshore areas south of Hainan Island, Northern South China Sea" Journal of Oceanology and Limnology, 18 (2): 132-139

Appendix 1: Surface Tension Effects on Waves

A1.1 Surface tension and free surface boundary conditions

When a liquid is in contact with another substance, there is a free interfacial energy present between them. This appears to contradict the principle of conservation of mechanical energy at the interface that states that the rate of work done by the fluid at the interface must be identical to the rate of work received by the other substance, i.e. the mechanical energy cannot be stored at the boundary. This apparent contradiction is because this interfacial energy cannot be described based on the continuum hypothesis but arises from the molecular-level dynamics, i.e., the interfacial energy is associated with the difference between the inward attraction of the molecules in the interior of each phase and those at the surface of contact. Let us consider a soap film that is stretched linearly with a distance dx; hence the work done in stretching the film is γLdx, where γ is the surface tension (force per unit length) and L is the width of the film. This work could be written as γdA where $dA=Ldx$. Therefore, instead of the quantity, force per unit length, the surface tension γ can be interpreted as an energy per unit area and the surface tension is often called surface free energy. The term "surface tension" implies that a liquid surface is extended by stretching the molecules on the surface, while the term "surface free energy" implies energy is required to form more surface by bringing molecules from the interior of the liquid to the surface (Adamson, 1990).

Consider small liquid-gas interfaces identified by two orthogonal elements ξ and ζ on the surface, Figure A1.1. Since the surface is small enough, the two radii of curvature R_1 and R_2 can identify the curvatures of the surface, which are in two normal plane sections at right angles to one another.

Hence, ξ and ζ are regarded as elements of the circumference of circles with radii R_1 and R_2. Suppose the surface is displaced by a small amount $d\eta$ outward, the change in area is:

$$\delta A = (\xi + d\xi)\cdot(\zeta + d\zeta) - \xi\cdot\zeta = \xi\cdot d\zeta + \zeta\cdot d\xi \qquad \text{(A1.1)}$$

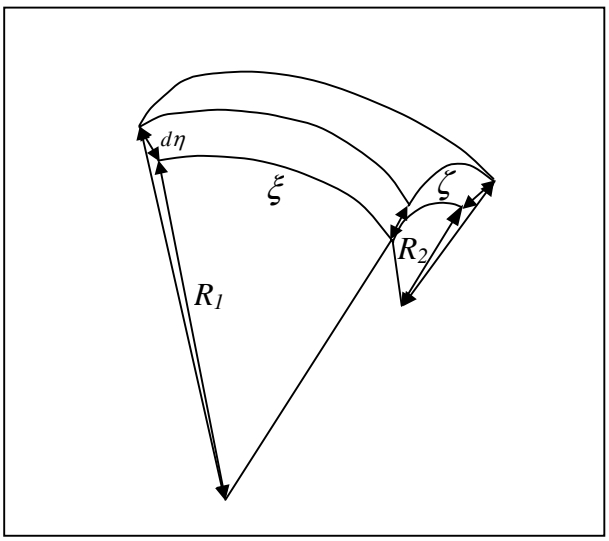

Figure A1.1

The work done in changing the area by surface-tension force is:

$$Work_{\gamma} = \gamma \cdot \delta A = \gamma \cdot (\xi \cdot d\zeta + \zeta \cdot d\xi) \tag{A1.2}$$

while the work done by the pressure difference, ΔP, between the two media is:

$$Work_{p} = \Delta P \cdot \xi \cdot \zeta \cdot d\eta \tag{A1.3}$$

From Figure A1.1 the following relation by similar triangles can be obtained:

$$\frac{\xi + d\xi}{R_1 + d\eta} = \frac{\xi}{R_1} \Rightarrow d\xi = \frac{\xi \cdot d\eta}{R_1} \tag{A1.4}$$

and, similarly

$$\frac{\zeta + d\zeta}{R_2 + d\eta} = \frac{\zeta}{R_2} \Rightarrow d\zeta = \frac{\zeta \cdot d\eta}{R_2} \tag{A1.5}$$

If the surface is at equilibrium, the works A1.2 and A1.3 must balance. Substituting A1.4 and A1.5 in A1.2 and equating A1.2 and A1.3 yields:

$$\Delta P = \gamma \cdot \left(\frac{1}{R_1} + \frac{1}{R_2} \right) \tag{A1.6}$$

This relationship is called Laplace's formula. Note that for a plane surface, *ΔP*, vanishes since the two radii become infinity, i.e., there is no pressure discontinuity across a plane surface.

The expression $\frac{1}{2} \cdot \left(\frac{1}{R_1} + \frac{1}{R_2} \right) = \frac{1}{2} \cdot \frac{1}{R}$ is called mean curvature radius and it could be demonstrated that for a surface of the form $z = \eta(x, y, t)$, 1/R can be expressed as:

$$\frac{1}{R} = -\frac{\eta_{xx} \cdot (1 + \eta_y^2) + \eta_{yy} \cdot (1 + \eta_x^2) - 2 \cdot \eta_{xy} \cdot \eta_x \cdot \eta_y}{(1 + \eta_x^2 + \eta_y^2)^{\frac{3}{2}}} \tag{A1.7}$$

For the case of a two-dimensional wave, $z = \eta(x, t)$, equation A1.7 simplifies to:

$$\frac{1}{R} = -\frac{\eta_{xx}}{(1 + \eta_x^2)^{\frac{3}{2}}} \tag{A1.8}$$

Assuming the equilibrium condition A1.8 to be valid, the dynamic boundary condition becomes:

$$[\![\tau_{ij} \cdot \bar{n}]\!] = \gamma \cdot \left(\frac{1}{R_1} + \frac{1}{R_2} \right) \cdot \bar{n} \tag{A1.9}$$

where the double brackets means the jump of tension across the free surface.

A1.2 Effects of surface tension on linear waves

For the case of a non-viscous fluid, the same dynamic condition is obtained for the three principal directions: $p = -\gamma \cdot \frac{1}{R}$,

where p is the pressure relative to the atmospheric pressure. If the flow is non-rotational, a velocity potential, ϕ can be defined and the relative pressure on the free surface can be obtained from the Bernoulli equation and the dynamic free surface boundary condition becomes:

$$-\frac{\partial\phi}{\partial t}-\gamma\cdot\frac{1}{R}+\frac{1}{2}\cdot\left[\left(\frac{\partial\phi}{\partial x}\right)^2+\left(\frac{\partial\phi}{\partial y}\right)^2+\left(\frac{\partial\phi}{\partial z}\right)^2\right]+g\cdot z=C(t)\ ;\ in\ z=\eta(x,y,t) \qquad \text{(A1.10)}$$

The linearized form of the dynamic free surface boundary condition is obtained neglecting all 2nd order terms from equation A1.2.1:

$$-\frac{\partial\phi}{\partial t}-\gamma\cdot\left(\frac{\partial^2\eta}{\partial x^2}+\frac{\partial^2\eta}{\partial y^2}\right)+g\cdot z=C(t)\ ;\ in\ z=\eta(x,y,t) \qquad \text{(A1.11)}$$

When this dynamic free surface boundary condition is applied to the solution of Laplace equation for linear waves of wave number k over horizontal bottom of depth h, the following dispersion relationship is obtained:

$$C^2=\frac{g}{k}\cdot\left(1+\gamma\cdot\frac{k^2}{\rho\cdot g}\right)\cdot\tanh(k\cdot h) \qquad \text{(A1.12)}$$

It can be seen that, at first approximation, the effect of the surface tension is to increase the wave celerity for all wave frequencies. For the case of deep-water waves, equation A1.12 simplifies to:

$$C^2=\frac{g}{k}+\frac{\gamma\cdot k}{\rho} \qquad \text{(A1.13)}$$

Equation A1.2.4 shows that the effect of surface tension increases as the wavelength decreases (increasing k). Equation A1.2.4 shows also that there is a minimum of celerity for the following wave number:

$$k_m=\sqrt{\frac{g\cdot\rho}{\gamma}} \qquad \text{(A1.14)}$$

For typical values in the sea g = 9.81 m/s^2, γ = 0.074 N/m and ρ = 1025 Kg/m^3, minimum celerity occurs for k = 368.62 m^{-1} or for a wave period of 0.1 seconds.

Figure A1.2 shows the relation between the terms of gravity and surface tension of equation A1.13 in the case of small amplitude deep-water waves. It can be seen that for wave periods over 0.2 s, the contribution of surface tension term to the celerity is negligible.

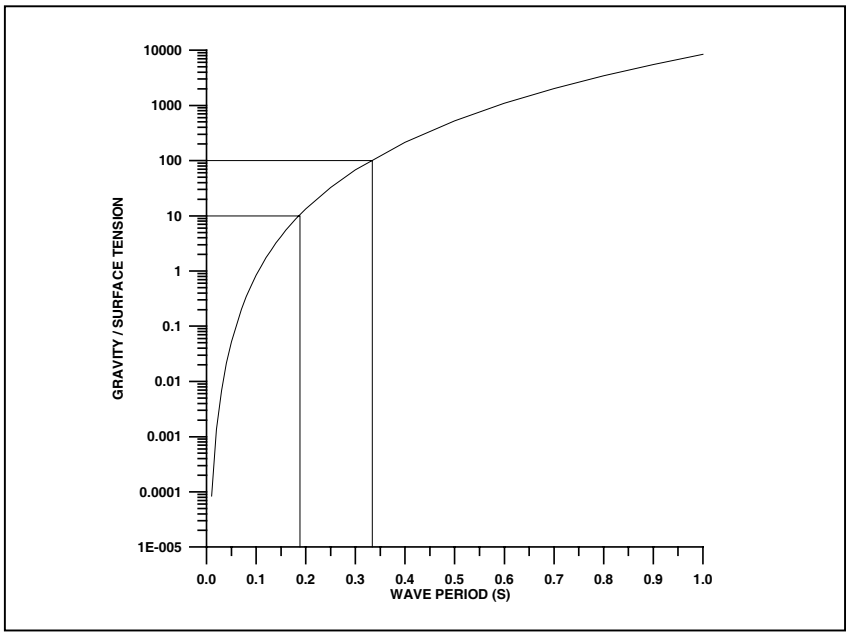

Figure A1.2. Relation between the terms of gravity and surface tension of equation (A1.2.4) in the case of small amplitude deep-water waves.

A1.3 Effect of surface tension on turbulent free surface flow

In the turbulent phase of the breaking process, a substantial amount of propagating wave energy is transferred to turbulent motions in the fluid local to the breaking crest. The turbulent motion is, of course, at the core of the importance of breaking because is responsible for mixing of the free surface, enhanced heat and mass transfer, and dissipation of mechanical energy. Unfortunately, the difficulties in performing theoretical, numerical and experimental studies of the turbulent phase of the breaking process are greater than in the earlier phases of breaking. These difficulties centre on dealing with the free surface, which can undergo large and partially random motions including those that generate droplets and bubbles.

Brocchini & Peregrine (unpublished) have used energy arguments to define several types of turbulent free-surface motion. The theory focuses on whether a given flow has sufficient turbulent kinetic energy to overcome the stabilizing effects of gravity and surface tension at the characteristic turbulent length scale. In turbulent spilling breakers, as the length of the gravity wave and the intensity of breaking increase, the free surface motions ranges from cases in which surface tension is dominant and gravity unimportant, where a single continuous surface exists with smooth round bumps, to cases with very strong turbulence, where gravity and surface tension are overcome by the kinetic energy of the fluid motion and the surface breaks up into drops and bubbles. Unfortunately, at the present time, the most precise experimental and numerical tools available can only be used in cases where the surface motion is relatively mild. Because of this limitation and the expense of operating large experimental facilities, our detailed knowledge of the breaking turbulent flow fields comes from the study of short-wavelength and/or relatively weak breakers.

In the field of wave breaking modelling, Dimas (1997) and Dimas & Fialkowski (2000) have developed a technique called Large Wave Simulation (LWS). As a demonstration of the technique, two-dimensional computations of wave breaking on a free-surface shear layer without surface tension are presented. When breaking is approached, the wave profile is

smooth, with smaller slopes than the direct numerical simulations and the calculation continues past the point where the direct simulation fails. The effect of breaking appears in the resolved scales as a strong vortex that develops just below the free surface on the front face of the wave.

Experimental studies of mechanically generated waves in deep water have also revealed interesting details of the dynamics of turbulent spilling breakers.

In Rapp and Melville (1990) study, several of the overall effects of breaking events including the loss of excess momentum flux and the production of surface currents were measured for $0.95 \leq L_c \leq 2.02$ m, where L_c is the wavelength obtained from the linear wave theory using the central frequency of the focused wave packets used to generate the breakers. The loss of excess momentum flux was found to range from 10% for spilling breakers to 25% for plunging breakers.

The details of the crest shape and flow field in very gentle spilling breakers, $0.77 \leq L_c \leq 1.18$ m, were reported in Duncan *et al.* (1994, 1999). The turbulent phase of the breaking process started when the toe begun to move down the wave face, see Figure 4.2.1. The toe quickly accelerated to a constant velocity whose vertical component was 0.135 times wave phase speed.

This is in contradiction to the theoretical model of Longuet-Higgins & Turner (1974), which predicted constant acceleration of the toe. The discrepancy might be due to the dominance of surface tension effects in the experiment, which are not included in the model, or the fact that in the experiments the slope of the wave face was changing in time while the model assumes constant slope. The behaviour of the ripples generated downstream of the toe after it began to move downslope was also observed in the experiments. As can be seen from the profile history in Figure 4.2.1, the ripples are generated with relatively short length at the toe and initially are nearly fixed in position relative to the crest. After generation their length increases as the move downstream with increasing speed. Flow field measurements using PIV during this process showed a rapid increase in circulation as a vortical region spread along the surface starting at the toe and extending back to the crest before the measurements ceased. A plot of a vorticity field shortly after the toe motion began is given in Figure A1.11.

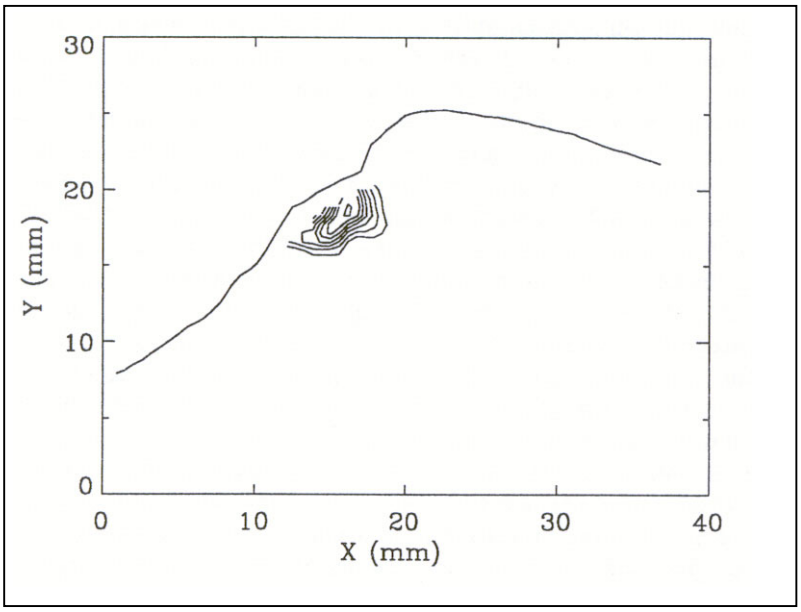

Figure A1.3. Vorticity field in a weak spilling breaker generated mechanically by the dispersive focusing technique. The average frequency of the wave packet is 1.42 Hz which, by linear theory, corresponds to a wavelength of 0.77 m. The vorticity field was measured shortly after the toe began to move down the wave face. The vorticity interval between contours is 40 s^{-1}. From Quiao & Duncan (unpublished).

The above results support the notion that the surface ripples are manifestations of local subsurface vortices that are generated on the shear layer extending from the toe and them are swept downstream as the shear layer grows in length.

Appendix 2: Effects of Surface Tension on Breaking Waves

When waves increase their steepness, the mean curvature radius in the crest decreases, thus increasing the surface-tension effects. Stokes (1880) analysis of deep-water periodic waves of maximum amplitude predicted a maximum wave steepness of $ak = 0.4432$ ($a = H/2$ or wave amplitude) with a sharp crest forming an angle between forward and backward slopes of 120º. This finding has been considered in the past as a model for breaking. However, it is most unlikely that such a flow can ever be realized, since uniform wave fields of much smaller steepness are subject to intrinsic instabilities, which may lead to breaking. Melville (1982) has shown experimentally that for wave steepness below approximately 0.3, two-dimensional uniform wave trains are unstable to two-dimensional Benjamin-Feir instabilities, which ultimately lead to breaking, while at larger steepness rapid three-dimensional instabilities dominate. Numerical solutions have shown that uniform wave trains with steepness as small as 0.1 may evolve to breaking following Benjamin-Feir instability (Dold & Peregrine, 1986). In conclusion, stability analyses of uniform wave trains have demonstrated the possibility of various breaking mechanisms for wave steepness less than 0.4432 (Longuet-Higgins *et al.,* 1994) if sufficient space is given.

Laboratory experiments by a number of authors (Bonmarin, 1989) have shown that deep water breaking waves may occur for values of wave height H and period T having a dimensionless wave height parameter H/gT^2 as small as 0.01, which is to be compared with a value of 0.2 for Stokes limiting wave steepness[1]. However, there is much scatter in the data. Although global measures of the steepness at breaking (ak, H/gT^2) may be quite modest, the local slope may become infinite, especially in overturning surfaces that entrain air.

Deep water waves may break as a result of constructive interference, wave-wave, wave-current an perhaps wind-wave interactions. The dispersion properties of surface waves and their directional distribution on the ocean surface leads to modulation of wave envelope. In the simplest case of deep-water linear wave propagation in one direction, envelope and wave energy travels at the group speed $C_g = \sigma/2k$ which is half the linear phase speed, so that wave crests enter the rear of the group and exit at the front. Donelan *et al.* (1972) observed the consequences of this process with waves periodically breaking as they passed through the group. Dispersion can lead to focusing of wave energy in a relatively small region, with the result that waves break in an unsteady manner. This can be produced in laboratory by first generating high-frequency waves followed by lower-frequency waves and then adjusting the rate of change of frequency according the linear group velocity to give focusing at a point down the channel. This process has proved useful to generate whitecaps in which the wave crest propagates forward and impacts on the surface below, entraining a volume of air that then breaks up into a cloud of bubbles (deep-water plunging breaker).

Recently, the constructive interference technique has been used to carefully investigate the threshold of breaking (Duncan *et al.*, 1994a,b). Flow visualization shows that at large crest curvatures a toe is formed on the forward face of the wave. The even higher curvature of the toe of the disturbance rapidly leads to the generation of parasitic capillary waves, which grow and evolve into a turbulent spilling region on the forward face of the wave, Figure A2.2. Longuet-Higgins & Cleaver (1994) have found that the formation of the initial toe is similar to an inviscid irrotational instability of the "almost highest" wave. The large curvature at the tip of the toe along with free-surface boundary conditions lead to the generation of vorticity

1 $ka = \frac{2\cdot\pi}{L}\cdot\frac{H}{2} = \frac{H}{g\cdot T^2}\cdot\frac{(2\cdot\pi)^2}{2} \approx 19.74\cdot\frac{H}{g\cdot T^2}$

associated with the capillary waves. This vorticity is then transported into the surface layers and, with the image vorticity in the surface, may resonate with free-surface modes (Longuet-Higgins, 1994).

Thus, criteria of breaking based on steepness or slope, consistent with Froude scaling, if valid at all, do not represent the effects of surface tension and viscosity and may result in scale-dependent breaking indexes.

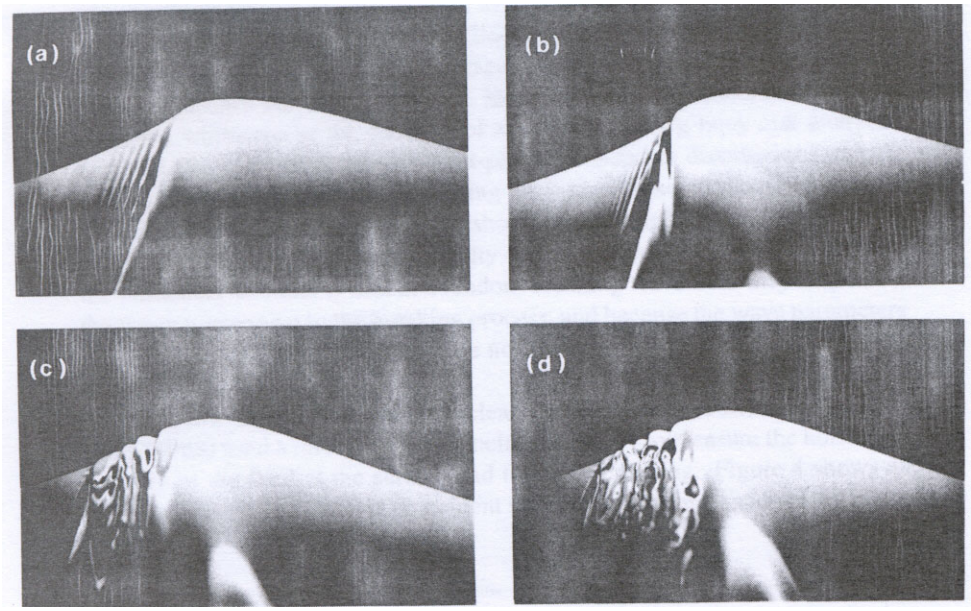

Figure A2.1. Generation of a gently breaking wave in the laboratory. Note the generation of the toe in the forward side of the crest (a) followed by the growth of parasitic capillary waves. (From Duncan et al. 1994b).

As shown in Figure A2.1, surface tension has rich effects on the strongly non-linear waves close to or at breaking. In Appendix A1 it is shown that the inclusion of surface curvature (with surface tension) means that the free-surface boundary condition itself requires further boundary conditions. Without surface tension deep-water waves can be modelled in the laboratory maintaining Froude similarity. As water is used in both the nature and in the laboratory, surface tension forces are not similar in laboratory than in prototype. That means that in a small-scale Froude model, surface tension forces can be much important in model than in prototype. These surface tension effects are more relevant near or at breaking, where non-linear deformation of waves increases surface curvature. As indicated by Duncan (2000) in his study of spilling breakers, for low wave steepness, the spilling process starts with the appearance of a rough surface, or in other cases a small jet, that creates a small turbulent path of fluid well above the mean water level. As the same wave is scaled to a shorter length, jet or droplet formation is influenced by surface tension and, for short waves, is replaced by a surface-tension-dominated ripple pattern on the forward face of the crest. This ripple pattern can break down to start the spilling process without overturning of the water surface. As the wave is scaled to even shorter wavelengths, the ripple pattern seems to remain at about the same physical size and therefore covers a larger fraction of the wave face. It is speculated that for very short waves (perhaps with lengths smaller than 10 cm) the initial turbulent region may cover a large fraction of the wave face at the time of its formation, and further growth by spilling may be minimal.

The effect of surface tension enters the equations of motion through the dynamic free-surface boundary condition, where the jump in pressure between air and water includes a term of the form T/R, where T is surface tension and R is local radius of curvature of free-surface in two-dimensional cases. The surface tension term increases in magnitude as the radius of curvature in the crest region decreases. For a given wave shape, curvature is proportional to wavelength so surface tension is more important for shorter waves.

At zero surface tension (equivalent to waves with long wavelengths) two-dimensional time-dependent numerical techniques predict the development and impact of a coherent jet in all cases. For a fairly wide range of breakers, though size of the jet varied relative to wavelength, jet shapes were nearly identical when scaled by the length of jet at the point in the profile evolution when the underside of the jet first became horizontal. Following Longuet-Higgins & Dommermuth (1997) it was shown that the crests have two unstable modes that result in the growth of a bulge on the forward face of the crest. The leading edge or toe of the bulge is located at a horizontal distance of 0.45 R_c (R_c= radius of curvature of the crest) ahead of the point of maximum elevation. It is important to note that since R_c scales with wavelength, L for a given wave shape (fixed R_c/L) the length scale of the bulge scales with L as well. The instability leads to the formation of a small jet that curls forward from the crest. Wave crest profiles from these calculations are shown in the upper part of Figure A2.2. As it can be seen from the figure, the jet is small and would impact with the wave face at a height of about 0.093 L above the mean water level while the crest is only 0.003 L above the impact height. Thus, the jet impact would lead to the formation of a spilling breaker.

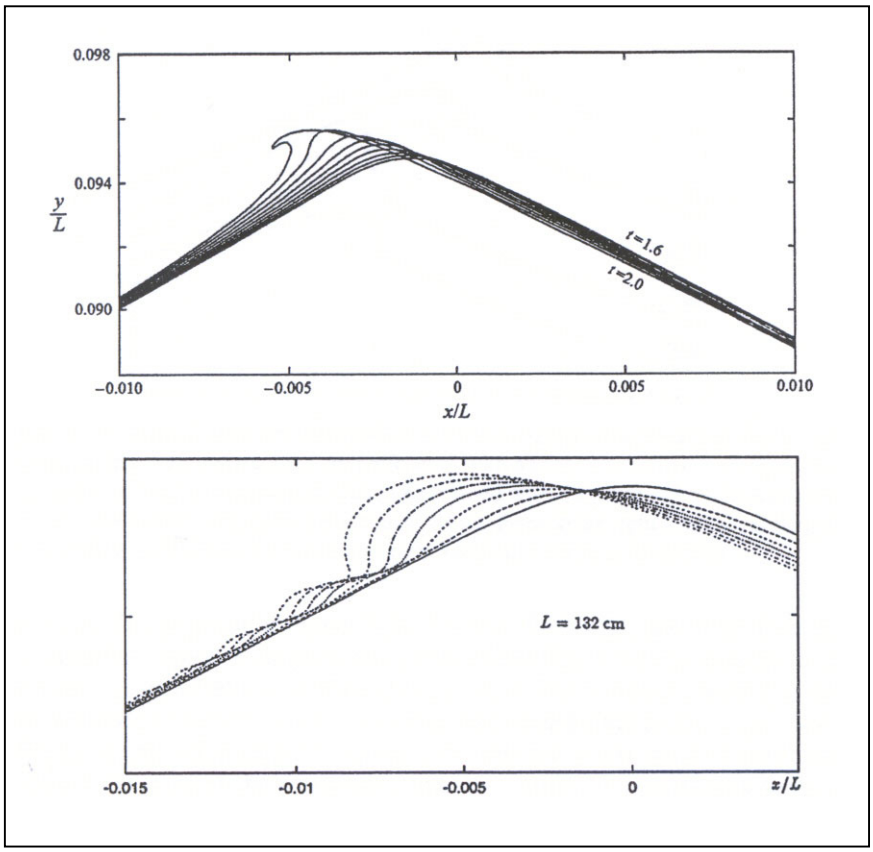

Figure A2.2. The non-linear development of the crest instability. (Top) $T = 0$, from Longuet-Higgins and Dommermuth (1997). (Bottom) $T = 73$ dyne/cm, wavelength $L = 132$ cm, from Longuet-Higgins (1997).

For short wavelengths, jet formation discussed above is modified by surface tension. These effects have been examined with boundary element calculations, theory and experiments. In the boundary element calculations presented by Tulin (1996), the effect of surface tension on the development of breaking due to side-band instabilities is explored. Selected results from this work are presented in Figure A2.3. The figure contains a series of profiles of waves of different length at times approaching breaking. When the wavelength is above about 2 m, breaking starts with the formation of a small plunging jet as it does when $T = 0$. As the wavelength decreases, surface tension forces become relatively larger and the jet tip becomes rounded. For wavelengths less than about 0.5 m, a bulge replaces the jet, and capillary waves appear upstream of the leading edge (toe) of the bulge. A set of profiles from Longuet-Higgins (1997) showing the effect of surface tension on the non-linear development of crest instability is given in the lower part of Figure A2.2. Note the similarity of these figures with photographs of Figure A2.1. Rather than forming a jet, the bulge from the crest instability continues to grow, and a train of capillary waves appears upstream of the toe. An important result from these calculations (not shown in Figure A2.2) is that in the presence of surface tension the non-dimensional length of the bulge, L_b/L, where L_b is the length of the bulge measured from the toe to the point of maximum elevation, increases as the wavelength decreases, while without surface tension, L_b/L is independent of wavelength.

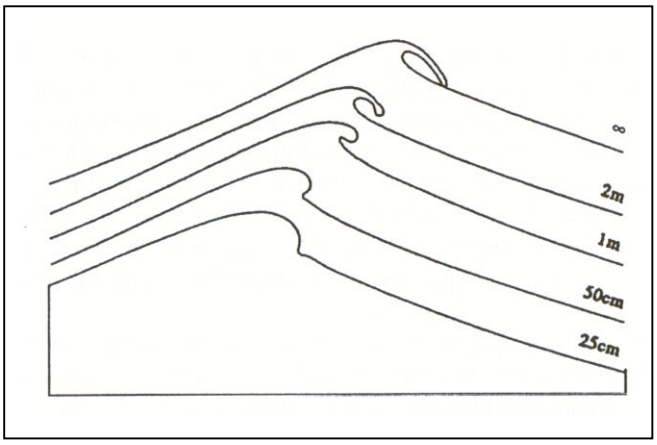

Figure A2.3. Numerical wavetank calculations for waves approaching breaking due to side-band instability. The calculations are performed with surface tension (T = 73 dyne/cm). Each profile is from a separate calculation performed with the same dimensionless wave-maker motion scaled to different frequencies; the numbers on the right are the wavelengths corresponding to the central frequency in each case. From Tulin (1996).

Ceniceros & Hou (1999) also used boundary element calculations to explore the effect of surface tension on the breaking process. In this work, a large-amplitude sinusoidal wave is initiated with an impulse that causes it to evolve to breaking in about 0.5 wave periods. In the absence of surface tension, the wave develops a large jet indicative of a strong plunging breaker. Results with surface tension for wavelengths ranging from about 0.01 to 1.54 m in water are given. At a wavelength of 0.77 m the jet still forms, but a bulge and capillary wave system can be seen on the underside of the jet near the tip. Perlin *et al.*, (1996) found similar capillary wave structures in an experimental study of plunging breakers with wavelengths of about 0.8 m. In the numerical calculations, as the gravity wavelength is decreased both the amplitude and wavelength of the capillary waves increase in a non-linear fashion, and the onset of the capillary waves occurs earlier in time.

Duncan *et al.*, (1994, 1999) performed an experimental study of spilling breakers generated mechanically by the dispersive focusing technique with L = 0.77 to 1.15 m. However, in these experiments only very weak breakers were investigated. A high-speed camera with a framing rate of 500 Hz was mounted on a carriage that moved with the wave to photograph the breaking events. The wave profile at the centreline of the tank was isolated by mixing the water with a small amount of fluorescent dye and illuminating it with a laser light sheet. For these weak breakers, a bulge-capillary wave system formed and the forward face of the crest as it steepened even though the gravity wavelengths were relatively long. A sample wave crest profile history is given in Figure A2.4 along with similar crest profile history for a wave generated by the side-band instability method with L = 0.41 m. The profiles for the focused wave are qualitatively similar to the theoretical and/or numerical predictions found in Longuet-Higgins (1997) and Tulin (1996) for times up to one of the profiles between those marked III and IV. The breaker generated by the side-band instability method also develops a bulge-capillary wave system, but the details are different than in the focused wave, perhaps owing to three-dimensional effects.

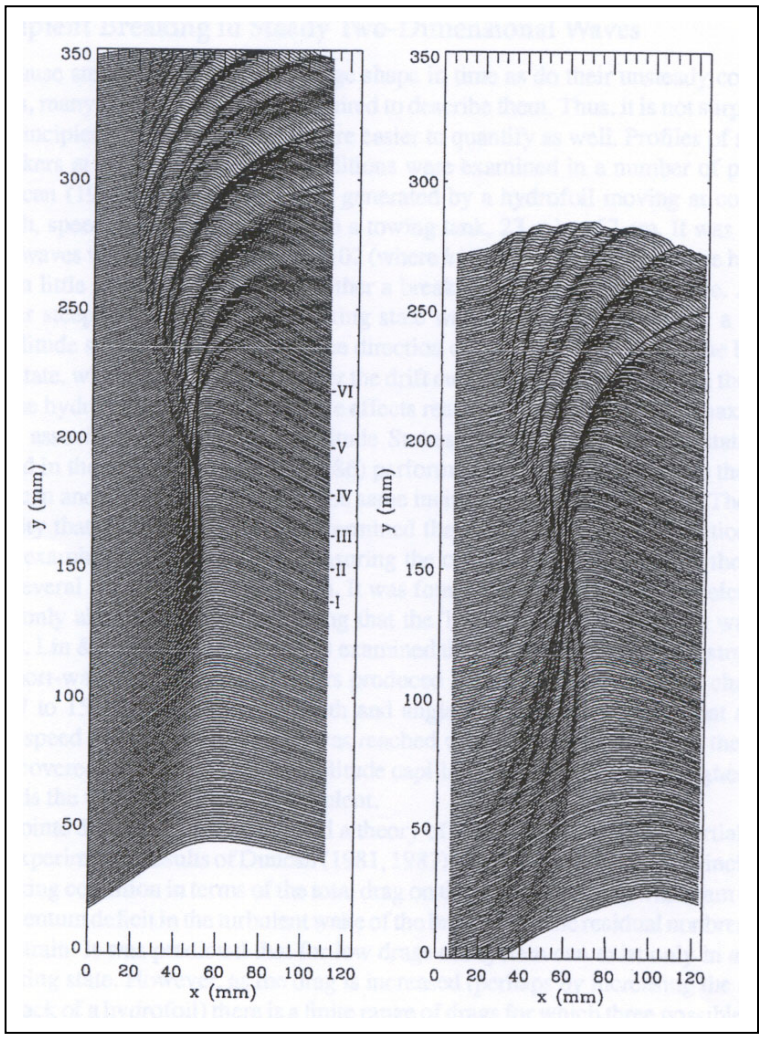

Figure A2.4. Crest profile of spilling breakers that are dominated by surface tension.

In Figure A2.4: Left: a very weak spilling breaker generated mechanically by the dispersive focussing method, from Duncan *et al.* (1999). The average frequency of the wave packet is 1.42 Hz. Right: a spilling breaker generated mechanically by the side-band instability method, from J.H. Duncan & G. Seer (unpublished). Main wave component frequency f = 1.953 Hz, initial wave steepness a_0k_0 = 0.275, where L_0 = 0.41 m and $k_0 = 2\pi/L_0$. In both plots each profile is taken from a single frame of a high-speed movie taken at 500 Hz in a reference frame moving with the crest. For clarity, each successive profile is raised by 1 mm above the preceding profile. The roman numerals at the right of the plot on the left refer to photographs in the original paper. From Duncan *et al.* (1999).

Appendix 3: Experimental Approaches to Scale Effects Associated to Wave Impacts

Some examples are present in literature, which propose correction of standard scale laws or different approaches to analyse wave impulsive loading on breakwaters.

Howarth *et al.* (1996) compared prototype results of pressures measured on a rubble mound breakwater protected with cob units (LaCollette, UK) with laboratory 2D results (scale 1:50). They confirm the assumption that simple Froude scaling leads to overestimation of magnitude (up to 500% !) and underestimation of rise times of impulsive pressures. After Froude scaling, they found the following empirical equation:

$$\frac{p_p}{\rho g} = \left(\frac{p_m}{\rho g}\right)^{0.684} \qquad \text{(A3.1)}$$

If entrained air affects impulsive loads, this does not necessarily mean that the ***impulse*** magnitude is affected. Pressure impulse is defined as $\int p(t)\,dt$, see Figure A3.1.

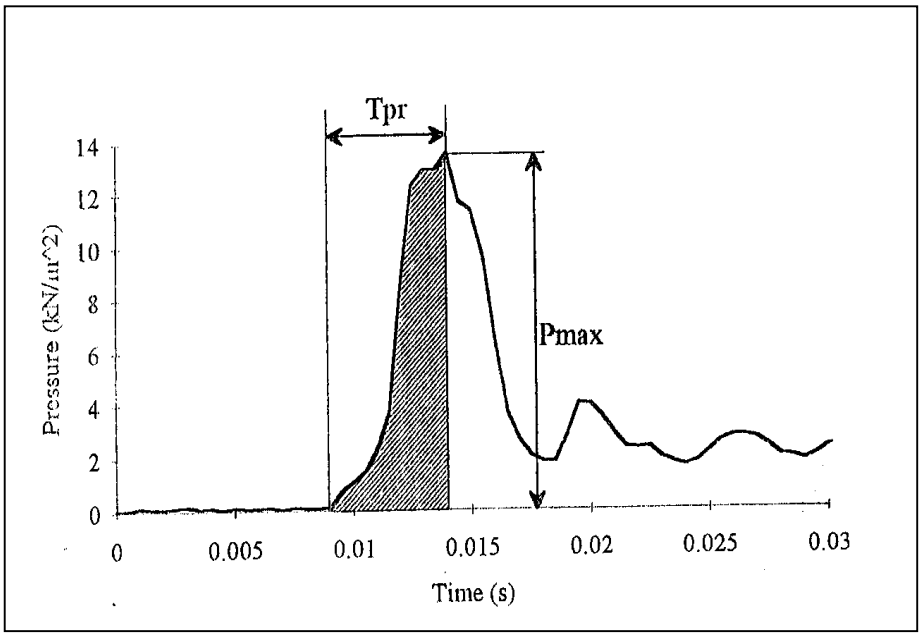

Figure A3.1. Definition of pressure rise impulse, after Walkden *et al*, 1996

Although aeration reduces water density, the wave mass remains the same due to bulking. It is therefore reasonable to think that wave impulse might be independent of the level of aeration, so possibly free of scale effects from model to prototype. For the analysis of pressure/force impulsive loads, Froude scaling could therefore be applied with recognised reliability on pressure impulse during impulsive events.

The above mentioned consistency of pressure/force impulses can be expressed as a relation between the maximum pressure/force recorded during an impulsive event and its duration t_d or its rise time t_r. Relations are of the form:

$$p_{\max} = \frac{A}{(t_d)^B} \qquad \text{(A3.2)}$$

where *A* and *B* are empirical coefficients.

Evidences can be found in literature of fitting equations of the same form as Equation A3.2. Coefficients *A* and *B* are highly sensitive to the different experiments (number of tests, experimental setup, test conditions). No clear relation between *A*, *B* and test variables can be found. In Figure A3.2 an example taken from Walkden *et al.* (1996) is shown, where small scale lab data are plotted together with large scale results.

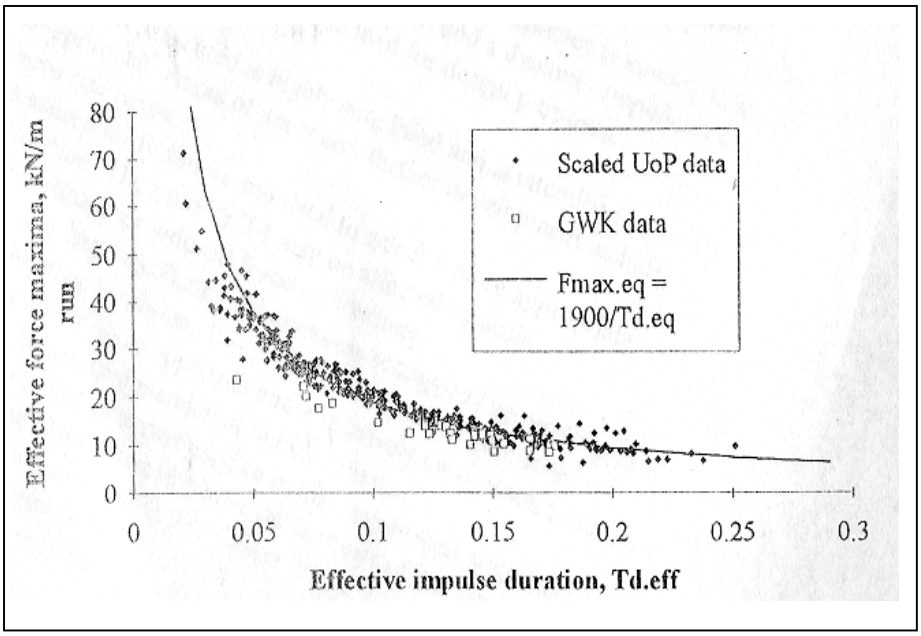

Figure A3.2. Maximum force versus impulse duration, after Walkden *et al*, 1996

Appendix 4: Boundaries for Sound Speed

Sea surface and sea floor affect underwater sound by providing (amongst others) a mechanism for:

- forward scattering and reflection loss (further complicated by refraction in the seabed);
- attenuation by a layer of bubbles at the surface and by sediment at the sea floor;
- noise generation at higher frequencies due to surface weather (at the sea surface) and at lower frequencies due to seismic activity (at the sea floor).

The mechanisms operating at the surface can be incorporated into mathematical models through the specification of "boundary conditions"; these can range from simplistic to complex, depending upon the sophistication of the model and the availability of information concerning the state of the sea surface and sea floor.

Although sea floor affects sound in ways similar to sea surface, the return of sound from the bottom is more complex than from the surface for several reasons: the bottom is more variable in composition; stratified with density and sound speed; composition and roughness can vary over relatively short horizontal distances.

Sea Surface Forward Scattering and Reflection Loss. As the sea surface roughens under the influence of wind, sound is scattered in the backward (giving rise to surface reverberation) and out-of-plane directions, and the intensity in the forward direction is accordingly reduced. A measure of the acoustic roughness of the sea surface is provided by the Rayleigh parameter R through, $R = 2k\alpha \sin\theta$ where $k=2\pi/\lambda$ is the acoustic wave number, λ is the acoustic wavelength, α is the root-mean-square (rms) amplitude of the surface waves and θ is the grazing angle relative to the horizontal plane. When $R < 1$, the sea surface is considered to be acoustically smooth, whereas for $R > 1$, the surface is acoustically rough. The sea surface is commonly modelled as a pressure release surface (Kinsler *et al.*, 1982); this is a condition in which the acoustic pressure at the air-water interface is nearly zero.

Sea Floor Forward Scattering and Reflection Loss. In the simplest model the bottom can be taken to be a homogeneous absorptive layer with a plane interface characterized by its density, sound speed and attenuation coefficient; in the case of sedimentary materials, all three of these parameters are determined by the porosity of the sediment. The major acoustical processes affecting interaction with the sea floor are: reflection in transmission of energy at the water-sediment interface; refraction of energy by positive sound speed gradient in the sediments; and attenuation within sediment.

Sea Surface Attenuation. The presence of bubble layers near the surface complicates further reflection and scattering of sound as a result of change in sound speed, resonant characteristics of bubbles and scattering by bubbly layers.

Sea Floor Attenuation. A compilation of measurements of sediment attenuation made by Hamilton (1980) over a wide frequency range, showed that the attenuation in natural, saturated sediments is approximately equal to 0.25kHz dB/m. Attenuation in sediments is several orders of magnitude higher than in pure water.

Ambient noise is the prevailing, unwanted background of sound at a particular location in the ocean at a given time.

Seismo-acoustic noise is referred to low frequency noise signals originating from the earth and the ocean. Orcutt (1988) three specific frequency bands, distinguished by the physics of the noise source: micro seism band (80mHz-3Hz) – resulting from non-linear wave-wave

interactions; noise-notch band (20-80mHz) – noise controlled by currents in the turbulent boundary layer near the sea floor; and ultra low-frequency band (<20mHz) – noise resulting from surface gravity waves.

Shipping noise can exhibit variability in both space and time; spatial variability is largely governed by distribution of shipping routes, whereas temporal variability is introduced, for example, by seasonal activity of the fishing fleets.

Marine ***bioacoustic*** signal sources are typically transient in nature and exhibit diverse temporal, spatial and spectral distributions; main contributors include shellfish, fish and marine mammals.

Established relationships have been produced between ***surface weather*** phenomena and ambient noise levels. Wind stress can be calculated from the measured ambient noise spectra (Shaw *et al.*, 1978). Ambient noise attributable to rainfall has also been used in an inverse fashion to provide estimates of oceanic precipitation (Nystuen, 1986). Pumphrey & Crum (1990) determined that the major cause of rain-generated sound is the production of bubbles upon water drop impact at the surface. These bubbles then oscillate with small amplitude and radiate as a dipole.

Appendix 5: Further References

Bullock G.N., Hewson P., Crawford A. & Bird. P.A.D. (2000) "Field and laboratory measurement of wave loads on vertical breakwaters" In: I J Losada (ed), Proceedings of the International conference Coastal Structures 99, vol 2, 613-622. A A Balkema: Rotterdam

Bullock G.N., Crawford A., Hewson P. & Bird. P.A.D. (2000) "Characteristics of wave impacts on a steep fronted breakwater" In: I J Losada (ed), Proceedings of the International conference Coastal Structures 99, vol 1, 455-464. A A Balkema: Rotterdam

Deane G.B. & Stokes M.D. (1999) "Air entrainment processes and bubble size distributions in the surf zone" Journal of Physical Oceanography, 29(7), 1393 – 1403

Farmer McNeil & Johnson (1993) "Evidence for the importance of bubbles in increasing air-sea gas flux" Nature, 361, 620-623

Garrett, C; Li, M; Farmer, D. (2000) "The connection between bubble size spectra and energy dissipation rates in the upper ocean" Journal of Physical Oceanography 30(9), 2163 – 2171

Johnson BD & Cooke RC (1979) BUBBLE POPULATIONS AND SPECTRA IN COASTAL WATERS: A PHOTOGRAPHIC APPROACH Journal of Geophysical Research, 84, 3761-3766

Klammer P., Kortenhaus A. & Oumeraci H. (1996) "Wave impact loading on vertical face structures for dynamic stability analysis" Proceedings of 25th International Conference on Coastal Engineering, Orlando, Florida, September 2-6, 2534-2546, Ed Billy L Edge, published by American Society of Civil Engineers, New York

Lamberti A. & Martinelli L. (1998) "Prototype measurements of the dynamic response of caisson breakwaters" Proc. 26th ICCE, Copenhagen, 22-26 June 1998, ASCE, pp. 1972-1985

Lamberti A. & Martinelli L. (2000) "Response to breaker impact of average European and Japanese caisson breakwaters" Proc. Int. Conf. Hydrodynamics IV (ICHD 2000), Yokohama, 665-670

Medwin H (1997) "IN SITU ACOUSTIC MEASUREMENTS OF MICROBUBBLES AT SEA" Journal of Geophysical Research, 82, 971-976

Medwin H & Breitz NJ (1989) "Ambient and transient bubble spectral densities in quiescent seas and under spilling breakers" Journal of Geophysical Research, 94, 12751-12579

Tirindelli M., Cuomo G., Allsop N.W.H & Lamberti A. (2002b) "Wave-in-deck forces on jetties and related structures" Paper submitted to ISOPE 2003 Conference, Honolulu